

Report reviewer1

Thanks for the detailed response. It indeed clarifies many things.

If I understand correctly, because the long sediment residence time in downstream grid cells near to the river mouth (Fig. S2), the sediment and C export from the river to the sea should be mainly controlled by the sediment and C budget in those downstream grid cells. Using the value of sediment export (1.6×10^7 tons yr^{-1}) and the value of C export (0.0095×10^{12} g C yr^{-1}), I calculated that the C density in those grid cells is only 6×10^{-5} g C g^{-1} . This is extremely low. I suspect that the simulated C density in other grid cells of large sediment residence times is also low.

Because the authors have explained that their focus is on the impact of soil erosion and deposition on land C dynamics in the revision, I actually agree that it is not important to make the simulated export of sediment and C to the sea match the observations. However, as said above, the problem of simulating C dynamics over floodplain cannot be ignored. I am not sure whether the problem is on the CE-DYNAM side or the ORCHIDEE side. Could you compare the surface layer C density in grid cells of long residence time between S0 and S2 to identify the cause? If it is on the CE-DYNAM side, further model improvement is needed.

Response: We thank the reviewer for his or her constructive comments. First, we would like to correct the POC and sediment export values of the Rhine. We mistakenly calculated the sediment bound POC export using the SOC concentration averaged over the whole soil profile, while we should have used the SOC concentration averaged over the topsoil layer (top 10cm) only as it is done in the routing of C in CE-DYNAM. After accounting for this oversight, we find that the new POC export at the Rhine outlet is around 2×10^8 g C yr^{-1} instead of the 9.5×10^8 g C yr^{-1} as written before. This new value is two orders of magnitude lower than the 2.6×10^{10} g C yr^{-1} given by the GlobalNEWS2 model (Mayorga et al., 2010), and is a result of the low simulated sediment export rate. The simulated sediment export value of the Rhine is 6472 tons yr^{-1} instead of the 1.6×10^7 tons yr^{-1} as written before. This value is also two orders of magnitude smaller than the 3.15×10^6 tons yr^{-1} that is found by Asselmann et al. (2003) or the 0.75×10^6 tons yr^{-1} simulated by Li et al. (2020). This is due to the fact that CE-DYNAM does not explicitly simulate rivers and streams. As a result, CE-DYNAM does not differentiate between eroded hillslope soil that reaches the water network in a relative short time, and the sediment that is first retained in the floodplains before it reaches the water network due to fluvial erosion. Instead the sediment and POC export rates in the model are only controlled by the sediment residence time of floodplain (alluvial) soil, which ranges between 0 and 1500 years, while the residence time of fine suspended sediment in rivers is usually much shorter (Wallbrink et al., 2002).

To account for the direct sediment flux from hillslopes to the water network, we would need to modify the floodplain sediment deposition ($f \cdot E$, see equation 4a), and differentiate between the sediment residence time of suspended sediment in rivers, and the residence time of alluvial deposits. However, the focus of this study was to model the full erosion-C loop, and not the sediment delivery to the water network. In a future study we aim to improve the sediment and POC export of the model by focussing on the suspended sediment fraction in the water network.

Furthermore, CE-DYNAM does not simulate fluvial erosion as a complex function of the channel geometry, riverbank erodibility and sheer stress (Droege et al., 1992), due to the lack of data on these parameters at the regional scale, and to keep a balance between model complexity and its computational ability. Also, our model does not resolve erosion of the deposited river sediment by flooding events. This simplified model concept for fluvial erosion contributes to the underestimation of

sediment export in floodplains. Finally, with the current model setup we do not account for large soil erosion events before 1850 or extreme precipitation events that may have a long-term effect on the sediment export rate of the Rhine. For the above-mentioned reasons it is hard to compare the sediment and POC export rates of our model with observations.

However, we find that the C density in the topsoil layers of floodplain soils located downstream of the Rhine and the C concentration of the POC flux are realistic. We find a C concentration of ~3.3% in the exported fine sediments. Abril et al. (2005) found a 5.5% POC mass fraction in suspended sediments for the Rhine. The C density of the topsoil layer of the floodplains in the downstream grid cells in the S2 simulations (S2, S2_min, S2_max) is on average 4.47 kg C m⁻², which falls within the range of the average C density of 5.13±1.3 kg C m⁻² measured by Hoffmann et al. (2013a) for floodplain overbank deposits. By comparison, the average C density of the topsoil layers of downstream grid cells in the S0 simulation is 12.78 kg C m⁻², which is an overestimation.

Changes to the manuscript: We updated the discussion about the sediment and POC export rates in section 4.2 (Model advantages and limitations) between lines 703 and 724 in the revised manuscript. We also updated the POC export rates in figure 8 and table 7.

Other comments

1) There are Hoffmann et al. (2013a & 2013b) in the references but only Hoffmann et al. (2013) is cited. Please clarify.

Response: Thank you for pointing this out. We cite both papers of Hoffmann as indicated in the references of the revised manuscript.

2) When checked Naipal et al. (2016), I noticed that simulated sediment storage can be an order of magnitude lower than the observations, even they show the similar scaling factors. How is the absolute value of simulated C storage compared with Hoffmann et al. (2013a)?

Response: The absolute value of C storage from the S2 simulations of the non-Alpine region of the Rhine for the year 2005 is in the range of 2.74-2.99 Pg of C, which is larger than the 1.7±0.6 Pg of C that Hoffmann et al. (2013a) measured. It should be noted that the ORCHIDEE model (S0 simulation) already overestimates the total SOC stock of the Rhine (2.43 Pg of C), when the initial conditions of the period 1850-1860 are used. Although this is in contrast to the findings of Hoffmann et al. (2013a), the difference in SOC stocks between floodplains and hillslopes from the S2 simulations is significantly better than the difference derived from the S0 simulation. We find that floodplains store 1.28-1.72 and hillslopes 1.7-2 Pg of C when erosion and deposition processes are taken into account, compared to 0.69 Pg of C for floodplains and 2.29 Pg of C for hillslopes when these processes are lacking. To be closer to the observational difference between floodplains and hillslopes we would need to consider the period before 1850, consider extreme climate events, and a higher plant productivity in floodplains. Furthermore, it should be noted that the sediment dynamics play a less important role in the total C storage compared to the NPP and soil respiration. Especially, if our study only considers the period 1850-2005 and not the entire Holocene like the study of Hoffmann et al. (2013a).

Changes to the manuscript: We include the comparison of the total SOC stocks in the discussion section 4.1 of the revised manuscript.

3) Eq. 6: Is this residence time equation universal in the world since the authors emphasized that the model would be applied globally?

Response: Yes, the equation should be applicable for large river basins worldwide such as the Rhine. However, the parameters of this equation are calibrated based on data from the Rhine. To be able to apply it on other river basins, it would be necessary to re-calibrate the parameters based on the specific sediment storage conditions of those basins.

Changes to manuscript: We include the following sentence in the revised manuscript after line 213 (section 2.3): ‘These constants will need to be calibrated based on local data of sediment ages before CE-DYNAM can be applied to other catchments globally.’

4) L436: Should be “lose” not “loose”.

Response: Thank you for pointing this out. We will correct this in the revised manuscript.

5) Could you explain what is net soil erosion? Is this the eroded sediment deposited to the floodplain fraction?

Response: The net soil erosion is the eroded sediment that leaves the hillslopes and is deposited to the floodplains.

Changes to manuscript: We will adjust line 310 in the revised manuscript (section 2.7) as following: ‘The change in C content due to net erosion (the eroded sediment/C that leaves the hillslopes after deposition) of the PFT-specific pools....’

6) Please define NPP and NEP before using abbreviations.

Response: NPP is the Net Primary Productivity and NEP is the Net Ecosystem Productivity. We will include these descriptions in the revised manuscript.

7) L548–449: Table 3 shows that the result of simulated net soil erosion is not good as described. Can be possibly related to my first comment?

Response: The estimation of the net soil erosion between our study and the study of Borrelli et al. (2018) is done in different ways, which may explain the difference in the results. In our study the deposition of sediment in hillslopes is explicitly calculated as a function of the slope, and vegetation type/cover. Borrelli et al. (2018) used the transport capacity concept (Van Rompaey et al., 2001). Both methods have their uncertainties when applied at large spatial scales. The method in our study has been designed and calibrated to be used at a large spatial scale, and at coarse resolution, while the method of Borrelli et al. (2018) was originally designed to be applied at spatial scales <100m, where the transport capacity coefficient needs to be calibrated with local data.

Changes to manuscript: We will include this explanation in the revised manuscript in section 3.1, after line 549.

8) L555-557: Sorry, I do not understand the mechanism. How can erosion-control and management practice affect this relationship?

Response: Indeed, erosion-control (EC) practices do not fully explain the difference in the relationships between soil and C erosion rates of the different studies. Thank you for pointing this out. EC practices reduce the overall erosion rates. Our study does not include them, and so our simulated erosion rates may be substantially larger in regions with EC. Figure 5 shows that our simulated erosion rates are in general larger than the erosion rates from Lugato et al. (2018), which may be explained by this mechanism. However, at the same time the C erosion rates of our study are lower than those of Lugato et al. (2018). This is likely due to the coarse spatial resolution of our underlying C-cycle -scheme, which is derived from the ORCHIDEE LSM.

Changes to manuscript: We will change lines 555-557 as following: ‘On the one hand, our study does not include erosion-control (EC) practices, leading to substantially larger simulated soil erosion rates in regions with EC. Figure 5 shows that our simulated erosion rates are in general larger than the erosion rates from Lugato et al. (2018), which may be explained by this mechanism. On the other hand, the C erosion rates of our study are lower than those of Lugato et al. (2018), due to the coarse spatial resolution of our underlying C-cycle -scheme derived from the ORCHIDEE LSM.’

9) Figure 3A: Why is the simulation missed in some bins?

Response: This is because the bins in figure 3a are based on the min-max erosion rates of Cerdan et al. (2010). For bin 8 where data is missing, there were no erosion rates from Cerdan et al. recorded. In our study the simulated maximum soil erosion rates were lower compared to Cerdan et al., likely due to the coarse spatial resolution of our model, therefore there is no data for bins with a high number.

Changes to manuscript: We will change line 1166 of revised manuscript as following: ‘ The x-axis represents bins or evenly spaced ranges between the minimum and maximum total yearly soil erosion rates of the Rhine derived from the data of (a) Cerdan et al. (2010), (b) Panagos et al. (2015), (c) Bug et al. (2014), and (d) Borrelli et al. (2018).’

We will also modify line 542 as following: ‘We find that the quantile distribution of the simulated gross soil erosion rates compares well to the distributions of other observational and high-resolution modelling studies (Cerdan et al., 2010, Panagos et al., 2015, Bug et al., 2014), although CE-DYNAM usually underestimates the very large soil erosion rates such as is found by Cerdan et al. (2010) (Fig 3A, B, C). This is due to the coarser spatial and temporal resolution of CE-DYNAM.’

Report reviewer2:

The manuscript presents a consistent and interesting study concerning carbon and erosion modelling. Authors presented the model CE-DYNAM which integrates sediment and C dynamics (structure, concepts, limitations and evaluation) applied at Rhine catchment scale during the period 1850-2005 AD. The study contributes to model soil organic carbon stock changes using a processbased model and to the evaluation of strategies to mitigate climate change at large scale.

Before publishing some minor revision should be addressed:

Line 61 "Most studies modeling soil erosion and its net effect on SOC dynamics at global scale" Please include references. Similarly in line 65

Response: We thank the reviewer for his or her constructive comments. We will include the following references to line 61 and 65 in the revised manuscript: 'Borrelli et al., 2018; Doetterl et al., 2012; Chappell et al., 2016; Lugato et al., 2018; Van Oost et al., 2007; Wang et al., 2017'

Line 107 Define Gross Primary Production

Response: We will define GPP in the revised manuscript.

Lines 132- 136 slope-length (describing the influence of topography on soil erosion risk.)

Changes to manuscript: We will include the following sentence to the revised manuscript: Note that the original Revised Universal Soil Loss Equation (RUSLE) (Renard et al., 1997) further includes a slope-length factor (L), which gives the length of a field in the direction of steepest descent, and a support practice factor (P), which accounts for management practices to mitigate soil erosion. These two factors have been excluded here, because their quantification still includes many uncertainties and is not practical for applications at regional to global scales.

The following sentence refers to slope-length? Revise: "These factors are a function of local manmade structures and management practices"

Response: This sentence refers to both L and P factors. The slope-length in agricultural steep landscapes is also largely controlled by the field size for example.

Changes to manuscript: We revise the sentence as: "These erosion factors are largely affected by local manmade structures (such as field size) and management practices"

Please clarify "we focus in this study on potential soil erosion and do not consider erosion-control practices"

Changes to manuscript: We modify this sentence as: 'In addition, we focus in this study on the potential effect of soil erosion on the C budget without erosion control practices. '

Line 153 similar catchments or not?
recommend using past tense lines 190, 194, 210

Response: Similar catchments is meant in line 153. We will include these corrections in the revised manuscript.

Line 191 "reducing the sediment transport from hillslopes to floodplains" this cannot be alid for some other regions then line 153 could be revised as follows: "should be also applicable for other similar catchments

Response: We will revise line 153 accordingly

Line 236 revise: “discretization scheme SOC scheme”

Line 397 contrasting

Line 468 Please specify to highlight the new contribution of the study

Changes to manuscript: We add the following sentence after line 468 in the revised manuscript: ‘In addition, the validation includes soil erosion data from new global soil erosion studies such as Borrelli et al. (2018) and Panagos et al. (2015).’

Line 479 Furthermore,

Line 518 avoid repetition “such as in our study. In our study”

Lines 519, 152, I suggest to include also in line 84

Response: We merge these lines in the last paragraph of the introduction of the revised manuscript.

Line 544 how about slope-length?

Response/Changes to manuscript: Thank you for pointing this out. We will add the following sentence in the revised manuscript: ‘This is due to the coarser spatial and temporal resolution of CE-DYNAM, and because we did not include the effects of the slope-length factor (L), while Cerdan et al. (2010) assumed a constant slope length of a 100m.’

Line 585 “started around 1910 AD” Include a reference/source

Changes to manuscript: We will add to line 585: ‘...that started around 1910 AD according to the data on landcover and land use (Peng et al., 2017; Fig 7B).’

Line 604 Figs

Line 659 chapter? Section

Line 671-674 Move to introduction

Response: We will revise this accordingly.

Line 679 I recommend using past tense as in line 689

Line 750 due to this limitation I suggest to revise the sentences in lines 87-88 and line 153 (globally); 689-690

Changes to manuscript: We will revise sentence 87-88 as following: ‘It should be noted here that the structure of CE-DYNAM is designed in a way that the model can be adapted easily to other large

catchments after calibrating the model parameters to the specific environmental conditions in those catchments.'

We will revise line 153 as following: However, the aim of this study is to present a carbon erosion model that should be also applicable for other large catchments.

Line 821 showed as in line 817. Please revise in the whole manuscript and keep the same tense

Response: We will revise this accordingly

CE-DYNAM (v1), a spatially explicit, process-based carbon erosion scheme for the use in Earth system models

Victoria Naipal^{1,2}, Ronny Lauerwald³, Philippe Ciais², Bertrand Guenet², Yilong Wang²

¹Ludwig-Maximilians University, Munich, Germany

²Laboratoire des Sciences des Sciences du Climat et de l'Environnement, CEA CNRS UVSQ, Gif-sur-Yvette 91191, France

³Department of Geoscience, Environment and Society, Université Libre de Bruxelles, Brussels, Belgium

Correspondence : Victoria Naipal (vnaipal24@gmail.com)

Abstract. Soil erosion by rainfall and runoff is an important process behind the redistribution of soil organic carbon (SOC) over land, hereby impacting the exchange of carbon (C) between land, atmosphere and rivers. However, the net role of soil erosion in the global C cycle is still unclear as it involves small-scale SOC removal, transport and re-deposition processes that can only be addressed over selected small regions with ~~complex measurements and models~~ **and measurements**. This leads to uncertainties in future projections of SOC stocks and complicates the evaluation of strategies to mitigate climate change through increased SOC sequestration.

In this study we present the parsimonious process-based Carbon Erosion DYNAMics model (CE-DYNAM) that links sediment dynamics resulting from water erosion with the C cycle along a cascade of hillslopes, floodplains and rivers. The model simulates horizontal soil and C transfers triggered by erosion across landscapes and the resulting changes in land-atmosphere CO₂ fluxes at a resolution of about 8 km at the catchment scale. CE-DYNAM is the result of the coupling of a previously developed coarse-resolution sediment budget model and the ecosystem C cycle and erosion removal model derived from the ORCHIDEE land surface model. CE-DYNAM is driven by spatially explicit historical land use change, climate forcing, and global atmospheric CO₂ concentrations affecting ecosystem productivity, erosion rates and residence times of sediment and C in deposition sites. The main features of CE-DYNAM are (1) the spatially explicit simulation of sediment and C fluxes linking hillslopes and floodplains, (2) the relative low number of parameters that allow running the model at large spatial scales and over long-time scales, and (3) its compatibility with global land surface models, hereby, providing opportunities to study the effect of soil erosion under global changes.

We present the model structure, concepts, limitations and evaluation at the scale of the Rhine catchment for the period 1850-2005 AD. Model results are validated against independent estimates of gross and net soil and C erosion rates, and the spatial variability of SOC stocks from high-resolution modeling studies and observational datasets. We show that despite local differences, the resulting soil and C erosion rates, and SOC stocks from CE-DYNAM are comparable to high-resolution estimates and observations at sub-basin level.

35
36 We find that soil erosion mobilized around 66 ± 28 Tg (10^{12} g) of C under changing climate and land use over the
37 non-Alpine region of the Rhine catchment, assuming that the erosion loop of the C cycle was in near steady-state by 1850.
38 This caused a net C sink equal to 2.1-2.7% of the Net Primary Productivity of the non-Alpine region over 1850-2005 AD.
39 This sink is a result of the dynamic replacement of C on eroding sites that increases in this period due to rising atmospheric
40 CO₂ concentrations enhancing the litter C input to the soil from primary production.

41

42 **Keywords.** soil erosion; regional carbon cycle; carbon sink; Rhine catchment; regional modelling

43

44 **1 Introduction**

45

46 Soils contain more carbon (C) than the atmosphere and living biomass together. Relatively small disturbances
47 (anthropogenic or natural) to soil C pools over large areas could add up to substantial C emissions (Ciais et al., 2013). With
48 the removal of natural vegetation and the introduction of mechanized agriculture, humans have accelerated soil erosion
49 rates. Over the last two to three decades, studies have shown that water erosion (soil erosion by rainfall and runoff)
50 amplified by human activities has substantially impacted the terrestrial C budget (Doetterl et al., 2012; Lal, 2003; Lugato et
51 al., 2018; Van Oost et al., 2007, 2012; Stallard, 1998; Wang et al., 2017). However, the net effect of water erosion on the C
52 cycle at regional to global scale is still under debate. This leads to uncertainties in the future projections of the soil organic
53 C (SOC) reservoir, and complicates the evaluation of strategies to mitigate climate change by increased SOC sequestration.
54 The study of Stallard (1998) was one of the first to show that water erosion does not only lead to additional C emissions
55 but can also sequester C due to the photosynthetic replacement of SOC at eroding sites and the stabilization of SOC in
56 deeper layers at burial sites. The study of van Oost et al. (2007) was the first to confirm the importance of the sequestration
57 of SOC by agricultural erosion at global scale using isotope tracers. Wang et al. (2017) gathered data on SOC profiles from
58 erosion and deposition sites and confirmed that water erosion on agricultural land that started from the early/middle
59 Holocene has caused a large net global land C sink. Other studies, however, argue that soil erosion is a net C source to the
60 atmosphere due to increased SOC decomposition following soil aggregate breakdown during transport and at deposition
61 sites (Lal et al, 2003; Lugato et al., 2018). Most studies modeling soil erosion and its net effect on SOC dynamics at global
62 scale, however, did not account for the full range of complex effects of climate change, CO₂ fertilization increasing
63 productivity and potentially soil C inputs, harvest of biomass, land use change, and changes in cropland management
64 (Borrelli et al., 2018; Doetterl et al., 2012; Chappell et al., 2016; Lugato et al., 2018; Van Oost et al., 2007; Wang et al.,
65 2017). In addition, models used at large spatial scales mainly focus on hillslopes and removal processes and neglect
66 floodplain sediment and SOC dynamics (Borrelli et al., 2018; Chappell et al., 2016; Lugato et al., 2018; Van Oost et al.,
67 2007). This can lead to substantial biases in the assessment of net effects of SOC erosion at catchment scale because
68 floodplains can store substantial amounts of sediment and C (Berhe et al., 2007; Hoffmann et al., 2013a,b). Studies

69 addressing long-term large-scale sediment yield from hillslopes and floodplains, such as Pelletier et al. (2012), do not
70 explicitly account for the redistribution of sediment and SOC over land.

71
72 Furthermore, soil erosion is one of the main contributors to particulate organic carbon (POC) fluxes in rivers and C export
73 to the coastal ocean. The riverine POC fluxes are usually much smaller than the SOC erosion fluxes, because only a small
74 fraction of eroded material is entering the river network, while POC losses occur in the river network and due to
75 decomposition and burial in floodplains and in benthic sediments (Tan et al., 2017; Galy et al., 2015). Therefore,
76 uncertainties in large-scale SOC erosion rates will lead to even larger uncertainties in lateral C fluxes between land and
77 ocean for past and future scenarios estimated by global empirical models on riverine C export (Ludwig and Probst, 1998;
78 Mayorga et al., 2010).

79
80 To address these knowledge gaps, we present a parsimonious process-based Carbon Erosion Dynamics Model
81 (CE-DYNAM), which integrates sediment dynamics resulting from water erosion with the SOC dynamics at the regional
82 scale. The SOC dynamics are calculated consistently with drivers of land use change, CO₂ and climate change by a
83 process-based land surface model (LSM), with a simplified reconstruction of the last century increase of crop productivity.
84 This modelling approach consists of a global sediment budget model coupled to the SOC removal, input, and
85 decomposition processes diagnosed from the ORCHIDEE global LSM in an offline setting (Naipal et al., 2018). **The main**
86 **aim of our study** is to quantify the horizontal transport of sediment and C along the continuum of hillslopes and
87 floodplains, and at the same time analyze its impacts on the land-atmosphere C exchange. We validate the new model with
88 regional observations and high-resolution modelling results of the Rhine catchment. It should be noted here that the
89 structure of CE-DYNAM is designed in a way that the model can be adapted easily to other large catchments **after**
90 **calibrating the model parameters to the specific environmental conditions in those catchments.** ~~and finally run globally~~ We
91 also discuss the model uncertainties and the sensitivity of the model to changes in key model parameters and assumptions
92 made. In the next sections we give a detailed overview of the CE-DYNAM model structure, the coupling of erosion,
93 deposition and transport with the coarse-resolution SOC dynamics of ORCHIDEE, model application and validation for the
94 non-Alpine region of the Rhine catchment, and its potentials and limitations.

95 96 **2 Methods**

97 98 **2.1 General model description**

99
100 CE-DYNAM version 1 (v1) is the result of coupling a large-scale erosion and sediment budget model (Naipal et al., 2016)
101 with the SOC scheme of the ~~land surface model~~ ORCHIDEE LSM (Krinner et al., 2005). The most important features of
102 the model are (1) the spatially explicit simulation of lateral sediment and C transport fluxes over land linking hillslopes and
103 floodplains, (2) consistent simulation of vertical C fluxes coupled with horizontal transport, (3) the low number of

104 parameters compared to other C erosion models that operate at a high spatial resolution (Lugato et al., 2018; Billings et al.,
105 2019) that allows running the model at large spatial scales and over time-scales up to several thousands of years, (4) the
106 generic input fields for application to any region or catchment, and (5) compatibility with ~~land surface models (LSMs)~~.

107
108 In the ORCHIDEE LSM, terrestrial C is represented by eight biomass pools, four litter pools and three SOC pools. Each of
109 the pools varies in space, time and over the twelve Plant Functional Types (PFTs). An extra PFT is used to represent bare
110 soil. ~~Natural and anthropogenic~~ and natural disturbances (as a result of climatic changes) to the C pools include fire, crop
111 harvest, changes to the Gross Primary Productivity (GPP), litterfall, autotrophic and heterotrophic respiration ~~as a result of~~
112 ~~climatic changes~~ (Krinner et al., 2005; Guimberteau et al., 2018). The C-cycle processes are represented by a C emulator
113 that reproduces for each PFT all C pools and fluxes between the pools exactly as in ORCHIDEE in absence of erosion. A
114 net land use change scheme is included in the emulator with mass-conservative bookkeeping of SOC and C input when a
115 PFT is changed into another from anthropogenic land use change (Naipal et al., 2018). The sediment budget model has
116 been added in the emulator to simulate large-scale long-term soil and SOC redistribution by water erosion using
117 coarse-resolution precipitation, land-cover and LAI data from Earth System Models (Naipal et al. 2015, 2016). The C
118 emulator including erosion removal was developed by Naipal et al. (2018) to reproduce the SOC vertical profile, removal
119 of soil and SOC starting from the topsoil, and compensatory SOC storage from litter input. As soil erosion is assumed not
120 to change soil and hydraulic parameters but only the SOC dynamics, the emulator allows substituting for the ORCHIDEE
121 model and performing simulations on time scales of millennia with a daily time step, which would be a very
122 computationally expensive or nearly impossible with the full LSM. The concept and all equations of the emulator are
123 described in Naipal et al. (2018). The following subsections describe the different components of the CE-DYNAM that
124 couples the C and soil removal scheme (Naipal et al., 2018) with the horizontal transport and burial of eroded soil and C
125 (Naipal et al., 2016).

126 127 **2.2 The soil erosion scheme**

128
129 The potential gross soil erosion rates are calculated by the Adjusted Revised Universal Soil Loss Equation (Adj. RUSLE)
130 model (Naipal et al., 2015), which is based on the original Revised Universal Soil Loss Equation (RUSLE) (Renard et al.,
131 1997) and part of the sediment budget model (Naipal et al., 2016) (Fig 1). In the Adj. RUSLE the yearly average soil
132 erosion rate is a product of rainfall erosivity (R), slope steepness (S), land cover and management (C_m) and soil
133 erodibility (K):

$$134
135 E = S * R * K * C_m \tag{1}$$

136
137 Note that the original RUSLE further includes a slope-length factor (L), which gives the length of a field in the direction
138 of steepest descent, and a support practice factor (P), which accounts for management practices to mitigate soil erosion.

139 These two factors have been excluded here, ~~because their quantification still includes many uncertainties and is not~~
140 ~~practical for applications at regional to global scales.~~The slope length (L) and support practice (P) factors, which are part
141 of the original Revised Universal Soil Loss Equation (RUSLE) model (Renard et al., 1997), have been excluded here
142 because their quantification still includes many uncertainties and is not practical for applications at regional to global
143 scales. These factors are largely affected by a function of local man-made structures (such as field size) and management
144 practices, which are difficult to assess for present day and whose changes over the past are even more uncertain. In
145 addition, we focus in this study on the potential effect of soil erosion on the C budget without ~~and do not consider~~
146 erosion-control practices.

147
148 Naipal et al. (2015) have developed a methodology to derive the ~~slope factor~~ S and the ~~erosivity factor~~ R factors from 5
149 arcmin resolution (5 x 5 arcminute raster) data on elevation and precipitation, hereby preserving the high-resolution spatial
150 variability in slope and temporal variability in erosivity. In the rest of the manuscript we will refer to X by X km/arcminute
151 raster cells always with X km/arcmin resolution. Despite the comparatively coarse resolution of the erosion model, the so
152 derived R factor was shown to compare well with the corresponding high-resolution product published by Panagos et al.
153 (2017). In the study of Naipal et al. (2016), where the soil erosion model was applied for the last millennium, the change in
154 climate was taken into account in the calculation of the R factor. For this study, we assume that the climate zones as defined
155 by the Koeppen-Geiger climate classification have not changed drastically since 1850 AD.

156

157 **2.3 The sediment deposition and transport scheme**

158

159 The sediment deposition and transport scheme have been adapted from the sediment budget model described by Naipal et
160 al. (2016), which has been calibrated and validated for the Rhine catchment (Fig 1). In the sediment budget model ~~rivers~~
161 ~~and streams are not explicitly simulated.~~ Instead each grid cell contains a floodplain fraction, which is needed to ensure
162 sediment transport between the grid cells (transport from one grid cell to another can only follow the connectivity of
163 floodplains). It should be noted that global soil databases do not identify floodplain soil as a separate soil class, although
164 national soil databases might. ~~Because we aim~~ However, the aim of this study is to present a carbon erosion model that
165 should be also applicable for other similar catchments ~~and eventually, globally.~~ Therefore, we followed a two-step
166 methodology to derive floodplains in the Rhine catchment. ~~For this purpose~~ ~~we used~~ using hydrological parameters and
167 existing data on hillslopes and valleys. First, grid cells were identified that consisted entirely out of floodplains. For this we
168 used the gridded global data set of soil at 5 arcminute resolution, with intact regolith, and sedimentary deposit thicknesses
169 of Pelletier et al. (2016) (Table 1), and identified lowlands and hillslopes based on soil thickness and depth to bedrock. The
170 lowlands were classified as grid cells that contain only floodplains and no hillslopes. Second, we calculated the floodplain
171 fraction (A_{fi}) of a grid cell i that has both hillslopes and floodplains as a function of stream length and width based on the
172 methodology developed by Hoffmann et al. (2007):

173

174 $A_{fl}(i) = L_{stream}(i) * W_{stream}(i)$ (2)

175

176 Where, L_{stream} is the stream length derived from the HydroSHEDS database (Lehner and Grill, 2013) (Table 1).

177

178 $W_{stream}(i) = a * A_{upstream}(i)^b$ (3)

179

180 Where, $A_{upstream}$ is the upstream catchment area, and a is equal to 60.8, and b is equal to 0.3.

181

182 The parameters a and b have been derived using from the scaling behavior of floodplain width as estimated from
 183 measurements on the Rhine (Hoffmann et al., 2007). The sediment deposition on hillslopes (D_{hs}) and floodplains (D_{fl}) is
 184 calculated as a function of the gross soil removal rates (E) according to Naipal et al. (2016) with the following equations:

185

186 $D_{fl}(i) = f(i) * E(i)$ (4a)

187

188 $D_{hs}(i) = (1 - f(i)) * E(i)$ (4b)

189

190 $f(i) = a_f * e^{\left(\frac{b_f * \theta(i)}{\theta_{max}}\right)}$ (5)

191

192 Where, f is the floodplain deposition factor at 8 km resolution that determines the fraction of gross eroded material
 193 transported and deposited in the floodplain fraction of a grid cell. a_f and b_f are constants parameters that relate f to the
 194 average topographical slope (θ) of a grid cell depending on the type of land cover. θ_{max} us the maximum topographical
 195 slope of the entire Rhine catchment.

196

197 The parameters a_f and b_f are chosen in such a way that f varies between 0.2 and 0.5 for cropland, reflecting the decreased
 198 sediment connectivity between hillslopes and floodplains created by man made structures such as ditches and hedges. For
 199 natural vegetation such as forests and natural grassland, a_f and b_f are chosen in a way that f varies between 0.5 and 0.8
 200 assuming that in these landscapes hillslopes and floodplains are well-connected. This assumption on the reduced sediment
 201 connectivity for agricultural landscapes is supported by several previous studies (Hoffmann et al., 2013a; de Moor and
 202 Verstraeten, 2008; Gumiere et al., 2011; Wang et al., 2015) on the effect of erosion on sediment yield (Hoffmann et al.,
 203 2013a; de Moor and Verstraeten, 2008; Gumiere et al., 2011; Wang et al., 2015). These studies showed that man-made
 204 activities on agricultural landscapes result in a trapping of eroded soil in colluvial deposition sites, reducing the sediment
 205 transport from hillslopes to floodplains. The model parameter f has been calibrated for the Rhine catchment before by in
 206 Naipal et al. (2016), where the ranges mentioned above are found to produce a ratio between hillslope and floodplain
 207 sediment storage that was comparable to observations. The studies of Wang et al. (2010; 2015) identified a range for the
 208 hillslope sediment delivery to be between 50 and 80 %, which is similar to the range in the (1-f) factor in our model. In each

209 case and within the defined boundaries, the slope gradient determines the final value of f . Eroded material that has not been
 210 deposited in the floodplains stays on the hillslopes and is assumed to be deposited at the foot of the hillslopes as colluvial
 211 sediment.

212
 213 The floodplain fractions of the grid cells are connected through an 8 km resolution flow routing network (Naipal et al.,
 214 2016), where the rivers and streams are indirectly included in the floodplain area but not explicitly simulated. By routing
 215 the sediment and C through the floodplain fractions of grid cells we lump together the slow process of riverbank erosion by
 216 river dynamics (time scale \approx a few years to thousands of years), and the rather fast process of transport of eroded material
 217 by the rivers (time scale \approx days). The rate by which sediment and SOC leave the floodplain of a grid cell to go to the
 218 floodplain of an adjacent grid cell is determined by the sediment residence time. The sediment residence time (τ) is a
 219 function of the upstream contributing area ($Flowacc$):

$$220$$

$$221 \tau(i) = e^{\frac{Flowacc(i)-a_r}{b_r}} \quad (6)$$

222
 223 The study of Hoffmann et al. (2008) showed that the majority of floodplain sediments have a residence time that ranges
 224 between 0 and 2000 years, with a median of 50 years. The constants a_r and b_r are chosen in such a way that basin τ varies
 225 between the 5th and 95th percentile of those observations, with a median for the whole catchment of 50 years. These
 226 constants are uniform for the whole basin. **These constants need to be calibrated based on local data of sediment ages**
 227 **before CE-DYNAM can be applied to other catchments.**

228
 229 Floodplain C storage follows the same residence time as sediment on top of the actual decomposition rate of C in a grid
 230 cell of ORCHIDEE. The routing of sediment and C between the grid cells follows a multiple-flow routing scheme. In this
 231 scheme the flow coming from a certain grid cell is distributed across all lower-lying neighbors based on a weight (W ,
 232 dimensionless) that is calculated as a function of the contour length (c):

$$233$$

$$234 W_{(i+k,j+l)} = \frac{\theta_{(i+k,j+l)} \times C_{(i+k,j+l)}}{\sum_{k,l=-1}^1 [\theta_{(i+k,j+l)} \times C_{(i+k,j+l)}]} \quad (7)$$

235
 236 Where c is $0.5 \times$ grid size (m) in the cardinal direction and $0.354 \times$ grid size (m) in the diagonal direction. (i, j) is the grid
 237 cell in consideration where i counts grid cells in the latitude direction and j in the longitude direction. $i+k$ and $j+l$ specify
 238 the neighboring grid cell where k and l can be either -1, 0 or 1. θ is calculated as the division between the difference in
 239 elevation (h) give in meters difference and the grid cell size (d), also in meters:

$$240$$

$$241 \theta_{(i+k,j+l)} = \frac{h_{(i,j)} - h_{(i+k,j+l)}}{d} \quad (8)$$

242

243 The sediment and C routing is done continuously at a daily time-step to preserve numerical stability of the model. More
244 detailed explanation of the methods presented in this section can be found in the study of Naipal et al. (2016).

245

246 **2.4 Litter dynamics**

247

248 The four litter pools in the emulator are an below- and an above- ground litter pool, each split into a metabolic and
249 structural pool with different turnover rates as implemented in ORCHIDEE (Krinner et al., 2005). The belowground litter
250 pools consist mostly out of root residues. Both the biomass and litter pools have a loss flux due to fire as incorporated in
251 ORCHIDEE by the Spitfire model of Thonicke et al. (2010). The litter that is not respired or burnt is transferred to the SOC
252 pools based on the Century model (Parton et al., 1987), which was modified by Naipal et al. (2018) to include a ~~and the~~
253 vertical discretization scheme for SOC ~~presented by Naipal et al., (2018)~~.

254

255 The vertical discretization scheme was introduced in the emulator to account for a declining C input and SOC respiration
256 with depth, and consists of 20 soil layers with each 10 cm thickness. The litter to soil fluxes from above-ground litter pools
257 are all attributed to the top 10 cm of the soil profile. The litter to soil fluxes from belowground litter pools are distributed
258 exponentially over the whole soil profile according to:

259

$$260 \quad I_{be}(z) = I_{0be} * \times e^{-r*z} \quad (9)$$

261

262 Where I_{0be} is the below-ground litter input to the surface soil layer and r is the PFT-specific vertical root-density attenuation
263 coefficient as used in ORCHIDEE. The sum of all layer-dependent litter to soil fractions is equal to the total litter to soil
264 flux as calculated by ORCHIDEE. The vertical SOC profile is modified by erosion and the resulting deposition fluxes,
265 which is discussed in detail in the following sections.

266

267 **2.5 Crop harvest and yield**

268

269 We adjusted the representation of crop harvest from ORCHIDEE by assuming a variable harvest index for C3 plants that
270 increases during the historical period as shown in the study of Hay (1995) for Wheat and Barley, which are also the main
271 C3 crops in the Rhine catchment. The harvest index is defined by the ratio of harvested grain biomass to above-ground dry
272 matter production (Krinner et al., 2005). In this study the harvest index increases linearly between 0.26 and 0.46 (Naipal et
273 al. 2018) consistent with the average values of Hay (1995). We also found that in certain cases the cropland ~~NPP~~ **Net**
274 **Primary Productivity (NPP)** was too high during the entire period of 1850-2005, especially in the early part of the 20th
275 Century. This is because the cropland photosynthetic rates were adjusted in ORCHIDEE to give a cropland NPP
276 representative of present day values that are higher than for the low input agriculture of the early 20th Century. To derive a
277 more realistic NPP for crop and barley in the Rhine catchment we used the long-term crop yield data obtained from a

278 dataset on 120000 yield observations over the 20th century in Northeast French Départements (NUTS3 administrative
 279 division) (Schauberger et al., 2018). According to the yield data assembled by Schauburger et al. (2018), yields in
 280 Northeast France (covers part of the Rhine catchment) for these crops increased fourfold during the last century. Note that
 281 crop residues like straw constituted a larger fraction of the total biomass in 1850 than in 2005, but those residues were
 282 likely collected and used for animal feed, housing fuel. We did not account for this harvest of residue in the simulation of
 283 SOC.

284

285 2.6 SOC dynamics without erosion

286

287 The change in the carbon content of the PFT-specific SOC pools in the emulator without soil erosion [awass](#) described by
 288 Naipal et al. (2018) (Fig 1) as follows:

289

$$290 \frac{dSOC_a(t)}{dt} = lit_a(t) + k_{pa} \times SOC_p(t) + k_{sa} \times SOC_s(t) - (k_{ap} + k_{as} + k_{0a}) \times SOC_a(t) \quad (10)$$

291

$$292 \frac{dSOC_s(t)}{dt} = lit_s(t) + k_{as} \times SOC_a(t) - (k_{sa} + k_{sp} + k_{0s}) \times SOC_s(t) \quad (11)$$

293

$$294 \frac{dSOC_p(t)}{dt} = k_{ap} \times SOC_a(t) + k_{sp} \times SOC_s(t) - (k_{pa} + k_{0p}) \times SOC_p(t) \quad (12)$$

295

296 Where, SOC_a , SOC_s , and SOC_p (g C m^{-2}) are the active, slow and passive SOC, respectively. The distinction of these SOC
 297 pools, defined by their residence times, are based on the study of Parton *et al.* (1987). The active SOC pool has the lowest
 298 residence time (1 - 5 years) and the passive the highest (200-1500 years). lit_a and lit_s ($\text{g C m}^{-2} \text{ day}^{-1}$) are the daily litter
 299 input rates to the active and slow SOC pools, respectively; k_{0a} , k_{0s} and k_{0p} (day^{-1}) are the respiration rates of the active,
 300 slow and passive pools, respectively; k_{as} , k_{ap} , k_{pa} , k_{sa} , k_{sp} are the coefficients determining the flux from the active to the
 301 slow pool, from the active to the passive pool, from the passive to the active pool, from the slow to the active pool and
 302 from the slow to the passive pool, respectively.

303

304 The vertical C discretization scheme in the emulator assumes that the SOC respiration rates decrease exponentially with
 305 depth:

306

$$307 k_i(z) = k_{0i}(z) \times e^{-re \cdot z} \quad (13)$$

308

309 Where k_i is the respiration rate at a soil depth z and re (m^{-1}) is a coefficient representing the impact of external factors, such
 310 as oxygen availability that decreases with depth. k_{0i} is the respiration rate of the surface soil layer for a certain SOC pool i .

311 The variable re is determined in such a way that the total soil respiration of a certain pool over the entire soil profile

312 without erosion is similar to the output of the full ORCHIDEE model. Detailed description of how this is done can be
313 found in the study of Naipal et al. (2018).

314

315 2.7 Net C erosion on hillslopes

316

317 In the model we assume that soil erosion takes place on hillslopes, and not in the floodplains due to the usually low
318 topographical slope of floodplains. The factor $(1-f)$ determines the fraction of the eroded soil that is deposited in the
319 colluvial reservoirs (Fig 1). Soil erosion always removes a fraction of the SOC stock in the upper soil layer depending on
320 the erosion rate and bulk density of the soil. The next soil layer contains less C and therefore at the following time-step less
321 C will be eroded under the same erosion rate. To account for this effect, the SOC profile evolution is dynamically tracked
322 in the model and updated at a daily time step, conform with the method of Wang et al. (2015). First, a fraction of the C
323 from each soil pool in proportion to the erosion height is removed from the surface layer. Then, at the same erosion rate,
324 SOC from the subsoil layer becomes the surface layer, maintaining the soil layer thickness in the vertical discretization
325 scheme. Similarly, the SOC from the subsoil later also moves upward one layer. The removal of C by erosion also triggers
326 a compensatory C sink due to the reduction in SOC respiration on eroding land. This compensatory C sink and reduced C
327 erosion over time will ultimately lead to an equilibrium state. The change in C content due to net erosion (the eroded
328 sediment/C that leaves the hillslopes after deposition) of the PFT-specific pools for hillslopes can be represented by the
329 following equations:

330

$$331 \frac{dSOC_{HSi}(z,t)}{dt} = k_E * \times SOC_{HSi}(z + 1, t) - k_E * \times SOC_{HSi}(z, t) \quad (14)$$

332

333 Where $dSOC_{HSi}(z,t)$ is the change in hillslope SOC of a component pool i at a depth z and at time step t . The daily net
334 erosion fraction k_E (dimensionless) is calculated as following:

335

$$336 k_E = \frac{f * \times \left(\frac{E}{365}\right)}{BD * \times dz} * \times EF \quad (15)$$

337

338 Where, E is the gross soil erosion rate ($t \text{ ha}^2 \text{ year}^{-1}$), f is the floodplain deposition factor, BD is the average bulk density of
339 the soil profile (g cm^{-3}), dz is the soil thickness ($=0.1 \text{ m}$), and EF is the C enrichment factor that is set to 1 by default. A
340 model sensitivity analysis will be performed (see section 4.3) with $EF > 1$ to represent a higher C concentration in eroded
341 soil compared to the original soil as a result of the selectivity of erosion. ~~$EF > 1$ represents a higher C concentration in
342 eroded soil compared to the original soil, due to the selectivity of erosion.~~

343

344 Hillslope erosion without the deposition term ~~This part of the model has been already applied at the global scale as part of~~
345 the C removal model presented by Naipal et al. (2018) ~~and is here extended with the deposition term detailed above.~~

346

347 2.8 C deposition and transport in floodplains

348
 349 The SOC-profile dynamics of floodplains are controlled by: (1) C input from the hillslopes, (2) C import by lateral
 350 transport from the floodplain fractions of upstream ~~neighboring~~ grid cells, and (3) C export to the floodplain fractions of
 351 downstream ~~neighboring~~ grid cells (Fig 1). First, the net eroded flux from the surface layer of the hillslope fraction of
 352 the grid cell ($k_E * SOC_{HS} (z=0)$) is incorporated in the surface layer of the floodplain. At the same deposition rate, the SOC
 353 of the surface layer of the floodplain is incorporated in the subsoil layer. Similarly, a fraction of the SOC of the subsoil
 354 layer is moved downward one layer. We will refer to this process as the ‘downward’ moving of C in the soil layer profile. It
 355 should be noted that C selectivity during transport and deposition is not taken into account here, meaning that the C pools
 356 of the deposited material are the same as the eroded material from the topsoil of eroding areas. At the same time a fraction
 357 of the C of the surface layer proportional to the sediment residence time (τ) is exported out of the catchment following the
 358 sediment routing scheme, resulting in the ‘upward’ moving of the C from the subsoil layers. This process represents the
 359 river bank erosion and resulting POC export by ~~the water network, although rivers. It should be noted that rivers and~~
 360 streams are not explicitly represented in the model. As we do not have information on the sub-grid spatial distribution of
 361 land cover fractions we first sum the exported C flux over all PFTs before assigning the flux proportionally to the land
 362 cover fractions of the receiving downstream-located ~~ying~~ grid cells. The C that is imported from the neighboring grid cells
 363 follows the same procedure as the deposition of eroded material, and results in a ‘downward’ moving of the C in the soil
 364 profile. The change in C content due to deposition and ~~routing river export/import~~ of the PFT-specific SOC pools for
 365 floodplains can be represented by the following equations:

$$366 \frac{dSOC_{FLi}(z,t)}{dt} = \left(\left(k_D + k_{i_{out}} \right) * SOC_{FLi}(z-1,t) \right) + \left(\frac{1}{(\tau*365)} * SOC_{FLi}(z+1,t) \right) - \left(\left(k_D + \frac{1}{(\tau*365)} + k_{i_{out}} \right) * SOC_{FLi}(z,t) \right)$$

367 , for $z > 0$ (16)

$$369 \frac{dSOC_{FLi}(0,t)}{dt} = \sum_{n=1}^{n=9} \left(k_{i_{out}}(n) * SOC_{FLi}(0,t)(n) \right) + \left(k_E * SOC_{HSi}(0,t) \right) + \left(\frac{1}{(\tau*365)} * SOC_{FLi}(1,t) \right) - \left(\left(k_D + \frac{1}{(\tau*365)} + k_{i_{out}} \right) * SOC_{FLi}(0,t) \right)$$

370 , for $z=0$ (17)

371
 372 Where n is the neighboring grid cell that flows into the current grid cell, $dSOC_{FLi}(z,t)$ is the change in floodplain SOC of a
 373 component pool i at a depth z and at time step t , and SOC_{HS} is the hillslope SOC stock. k_D is the deposition rate and equal
 374 to:

$$375 k_D = \frac{k_E * AREA_{HS}}{AREA_{FL}}$$

376 (18)

377
 378 Where $AREA_{HS}$ is the hillslope area and $AREA_{FL}$ is the floodplain area (m^2). $k_{i_{out}}$ is the import rate per C pool i from
 379 neighboring grid cells (dimensionless) and can be calculated as:

381

$$k_{i_{out}} = \frac{\sum_{n=1}^{n=9} (W * \frac{1}{t^{*365}} * AREA_{FL}(n))}{AREA_{FL}} \quad (19)$$

383

384 Where, W is the weight index of equation 7.

385

386 The first term of equation 16 represents the ‘downward’ moving of the incoming C related to the C deposition flux from
 387 the hillslope fraction of the grid cell and the lateral C import flux from the floodplain fractions of upstream neighboring
 388 grid cells. The second term represents the ‘upward’ moving of SOC related to the lateral C transfer to downstream
 389 neighboring grid cells. The third term of equation 16 represents the total C loss flux from the current soil layer z, which is a
 390 result of either the ‘upward’ or ‘downward’ moving of the C in the soil profile. The first term of equation 17 represents the
 391 incoming lateral C flux from the floodplains of the upstream neighboring grid cells. The second term represent the C
 392 deposition flux coming from the hillslope fraction of the grid cell. The third term represents the ‘upward’ moving of the
 393 SOC from the subsoil layer to the topsoil layer as a result of sediment/C routing. The last term of equation 17 represents
 394 the total loss of C from the topsoil layer, of which part is distributed across the neighboring grid cells downstream ($\frac{1}{(t^{*365})}$
 395), and another part is moved ‘downwards’ in the soil profile as a result of C deposition (k_D) and the incoming later C from
 396 upstream grid cells ($k_{i_{out}}$).

397

398 2.9 The land use change bookkeeping model

399

400 The land use change bookkeeping scheme includes the yearly changes in forest, grassland and cropland areas in each grid
 401 cell as reconstructed by Peng et al. (2017) (Table 1). Peng et al. (2017) derived historical changes in PFT fractions based on
 402 LUHv2 land use dataset (Hurtt et al., 2011), historical forest area data from Houghton, and present day forest area from
 403 ESA CCI satellite land cover (European Space Agency, ESA, 2014). By using different transition rules and independent
 404 forest data to constrain the changes in crop and urban PFTs they derived the most suitable historical PFT maps.

405

406 When land use change takes place, the litter and SOC pools of all shrinking PFTs are summed and allocated proportionally
 407 to the expanding PFTs, maintaining the mass-balance. In this way the litter pools and SOC stocks get impacted by different
 408 input and respiration rates for each soil layer. When forest is reduced, three wood products with decay rates of 1, 10 and
 409 100 years are formed and harvested. The biomass pools of other shrinking land cover types are transformed to litter and
 410 allocated to the expanding PFTs. For more details on the land use scheme are described in see the study of Naipal et al.
 411 (2018).

412

413 2.10 Study-Area

414

415 The model is tested for the Rhine catchment (Fig 2), which has a total basin area of about 185,000 km² covering five
416 different countries in Central Europe. Its large size is beneficial for the application of a coarse-resolution model such as
417 CE-DYNAM to study large-scale regional dynamics in the C cycle due to soil erosion. The Rhine catchment has a
418 contrasting ~~very interesting~~ topography, with steep slopes larger than 20% upstream in the Alps, and large, wide and flat
419 floodplains at the foot of the Alps, the upper Rhine and the lower Rhine. The floodplains store large amounts of sediment
420 and C that originate from eroding ~~originally was eroded from the steep hillslopes~~ upstream. These sediment storages
421 provide the ~~This makes it possible~~ to study the long-term effect of erosion on hillslope and floodplain dynamics.
422 Furthermore, the Rhine catchment has been experiencing different stages of land use change over the Holocene, with land
423 degradation dating back to more than 5500 years ago (Dotterweich, 2013). In contrast, during the last two decades there
424 has been a general afforestation and soil erosion has been decreasing. These land use changes and changes in erosion make
425 an interesting and important case to study the effect of anthropogenic activities on the C cycle in Europe.

426
427 In addition, the Rhine catchment has been the focus of many erosion studies providing observations on erosion and
428 sediment dynamics that can be used for model validation (Asselman, 1999; Asselman et al., 2003; Erkens, 2009; Hoffmann
429 et al., 2007, 2008, 2013a, 2013b; Naipal et al., 2016). The global sediment budget model that forms the basis for the
430 sediment dynamics scheme of CE-DYNAM has been validated and calibrated for the Rhine catchment with observations
431 on sediment storage from Hoffmann et al. (2013a) and the derived scaling relationships between sediment storage and
432 basin area (Naipal et al., 2016). Hoffmann et al. (2008, 2013a) did an inventory of 41 hillslope and 36 floodplain sediment
433 and SOC deposits related to soil erosion over the last 7500 years. The floodplain sediment observations consist mostly out
434 of organic material (gyttja, peat) and fine sediments (fine sand, loam, silt) in overbank deposits (Hoffmann et al., 2008).
435 These fine sediments are a result of long-term soil erosion on the hillslopes. Hoffmann et al. (2013a) found that the
436 sediment and SOC deposits were quantitatively related to the basin size according to certain scaling functions, where
437 floodplain deposits increased in a non-linear way with basin size while the hillslope deposits showed a linear increase with
438 basin size. We will use these relationships to validate the spatial variability in SOC storage of floodplains and hillslopes
439 simulated by CE-DYNAM. The scaling relationships have the form of a simple power law:

$$440$$
$$441 M = a * \left(\frac{A}{A_{ref}}\right)^b \quad (20)$$
$$442$$

443 Where M is the sediment storage or the SOC storage, a is the storage (Mt) related to an arbitrary chosen area A_{ref} , while b is
444 the scaling exponent.

445

446 **2.11 Input data and model simulations**

447

448 To create the C emulator that forms the underlying C cycle part of CE-DYNAM, we first ran the full ORCHIDEE model
449 for the period 1850-2005 at a coarse resolution of 2.5°degrees latitude and 3.75° degrees longitude, and output all C pools

450 and fluxes. The pools and fluxes were then archived together and used to derive the turnover rates to build the emulator.
451 The SOC scheme of the emulator that has been modified to account for soil erosion processes has been made to run at a
452 spatial resolution of 5 arcmin, similar to the original global sediment budget model. Then, we performed three main
453 simulations with CE-DYNAM for the Rhine catchment. Simulation S0: The baseline simulation or no-erosion simulation,
454 where SOC dynamics are similar to the full ORCHIDEE model. Simulation S1: The erosion -only simulation, where the
455 hillslopes erode and all eroded C is respired to the atmosphere without reaching the colluvial and alluvial deposition sites.
456 Simulation S2: The simulation with full sediment dynamics where hillslopes and floodplains are connected and can
457 ~~bury~~ store or loose C. We ran the emulator for 3000 years at a daily time step with the initial climate and land cover of the
458 period 1850-1860. To speed up the spin-up simulations we calculated the temporary equilibrium state of the floodplain
459 SOC pools every 10 years analytically. At the end of the spin-up period the floodplain SOC pools were close to
460 equilibrium, with a yearly change of less than 0.001% of the total floodplain SOC stock. Afterwards, we performed the
461 transient simulations for the period 1851-2005 at a daily time step with changing climate and land cover conditions, using
462 the equilibrium SOC stocks as baseline. To ensure a faster performance of CE-DYNAM we delineated the Rhine
463 catchment in seven large sub-basins ~~based on the flow direction~~ and ran the model in parallel for each of the sub-basins at a
464 daily timestep. After each year the sub-~~basin~~ catchments exchanged the lateral C fluxes with each other.

465
466 We also performed seven additional sensitivity simulations and four additional uncertainty simulations. Simulation S1_EF
467 and S2_EF are performed to test the model assumption of a C enrichment during erosion. Here, we changed the enrichment
468 factor EF to two, based on the study of Lugato et al. (2018). Simulations S2_Tmin and S2_Tmax are performed to test the
469 rate of C transport between floodplains. Here we modified the ~~mean~~ average sediment residence time for the Rhine
470 catchment to a minimum of 60 years (50 % lower than the current value), and to a maximum of 128 years (50% higher than
471 the current value), respectively. However, we kept the maximum sediment residence time at 1500 years. Simulations
472 S0_RM, S1_RM and S2_RM are performed to test the model assumption on crop residue management, where we assumed
473 that all above-ground crop litter is harvested.

474
475 For the uncertainty analysis we performed simulations S1_min and S2_min based on a minimum soil erosion scenario, and
476 S1_max and S2_max based a maximum soil erosion scenario. These soil erosion scenarios are ~~derived from~~ based on the
477 uncertainty ranges in the rainfall erosivity and land cover factors of the erosion model. All the model simulations are
478 summarized in table 2.

480 2.12 Validation methods and data

481
482 We performed a detailed model validation of the sediment and the C part of the model ~~according to~~ based on the following
483 steps: (1) validation of soil erosion rates using observational and high-resolution model estimates for Germany and Europe,
484 (2) validation of C erosion rates using high-resolution model estimates for Europe from Lugato et al. (2018), (3) validation

485 of the spatial variability of hillslope and floodplain C storage using observational results from Hoffmann et al. (2013a), (4)
486 validation of SOC stocks using observational data from a global soil database and a European land use survey.

487
488 The validation of the soil erosion module has been done before in the studies of Naipal et al. (2015, 2016). However, we do
489 it again in this study due to different input datasets. In addition, the validation includes soil erosion data from new global
490 soil erosion studies such as Borrelli et al. (2018) and Panagos et al. (2015). For the validation of gross soil erosion rates we
491 used the high-resolution model estimates from the study of Panagos et al. (2015), who applied the RUSLE2015 model at a
492 100 m resolution at European scale for the year 2010. Similarly to the Adj.RUSLE, The RUSLE2015 is also derived from
493 the original RUSLE model, with some modifications to the erosion factors model parameters L, C and P. The erosion
494 module of CE-DYNAM is also based on a modified version of the RUSLE (Adj.RUSLE) which, however, lacks the L
495 and P factors. It calculates the potential soil erosion rate under the assumption of no erosion control scenarios, in contrast to
496 RUSLE2015, which does represent erosion control practices. However, in contrast to our model, RUSLE2015 does
497 include the erosion factors *L* and *P*. Adj.RUSLE also differs from RUSLE2015 in the use of Furthermore, our model uses
498 more coarsely resolved input datasets (Table 1), for which the equations for the R and S factors have been modified. The
499 extensive validation of the Adj. RUSLE model in this study and previous studies (Naipal et al., 2015, 2016, 2018), shows
500 that despite its coarse resolution, it is applicable at the methodology works for large spatial scales. In contrast, RUSLE2015
501 uses largely similar equations as in the original RUSLE model presented in Renard et al. (1997). Thus, even though both
502 Adj.RUSLE and RUSLE2015 are derived from the same erosion model, the differences between the models are large,
503 which justifies and would justify our model comparison.

504
505 Furthermore, we used independent high-resolution erosion estimates from the study of Cerdan et al. (2010), available at a
506 1 km resolution at European scale, which were based on an extensive database of measured erosion rates under natural
507 rainfall in Europe. For the comparison we aggregated the high-resolution model results of both datasets to the resolution of
508 CE-DYNAM. We also used the potential soil erosion map of the Federal Institute for Geosciences and Natural Resources
509 of Germany (Bug and Stolz, 2014). This map presents the yearly average soil erosion rates at a 250 m resolution on
510 agricultural land derived from a USLE-based approach, with some modifications to the erosion factors and input data.
511 Before validating our model results we also aggregated these high-resolution erosion rates to the coarser resolution of our
512 model.

513
514 Validation of our net soil erosion rates is done based on the 100 m resolution net soil erosion rates derived with the
515 WATEM-SEDEM model (Borrelli et al., 2018). WATEM-SEDEM simulates soil removal by water erosion based on the
516 USLE approach, sediment transport and deposition based on the transport capacity. The model has been extensively
517 employed to estimate net fluxes of sediments across hillslopes at catchment- and regional-scales level.

518

519 For the validation of C erosion rates, we used the high-resolution model results from Lugato et al. (2018), where they
520 coupled the RUSLE2015 erosion model to the Century biogeochemistry model. These model results were available at a
521 resolution of 1 km, where each grid cell was composed of an erosion and deposition fraction. The C erosion rates provided
522 by Lugato et al. (2018) were multiplied with the erosion fraction of a 1 km grid cell. Then, the C erosion rates were
523 aggregated to the resolution of CE-DYNAM. Lugato et al. (2018) provided an enhanced and a reduced erosion-induced C
524 sink uncertainty scenario, based on different assumptions for C enrichment, burial and C mineralization during transport. In
525 CE-DYNAM the C erosion rates from simulation S1 are multiplied with the hillslope area to get the total C erosion flux of
526 a grid cell. As the study of Lugato et al. (2018) considers only agricultural areas, we considered only the crop fraction of a
527 grid cell. It should be noted that the SOC dynamics scheme of CE-DYNAM, which is derived from ORCHIDEE LSM, is
528 also based on the Century model. However, there are large differences between the Century model used by Lugato et al.
529 (2018) and the C dynamics scheme of ORCHIDEE used in this study. For example, in the Century model the crop
530 productivity is mediated by nitrogen availability, which is not the case in the ORCHIDEE version used for this study. The
531 Century model also includes some management practices such as crop rotations, which are not represented in ORCHIDEE.
532 The Century model runs at a much higher resolution and is calibrated for agricultural land, while ORCHIDEE also
533 simulates forest, grasslands and bare soil. In this way, the final SOC stocks derived with CE-DYNAM are also a result of
534 erosion from other land cover types and land use changes. This is an important feature for land use change, which is not
535 included in the Century model. Furthermore, the ORCHIDEE LSM has been used in many global intercomparisons and
536 extensively evaluated for C budgets (Mueller et al., 2019; Todd-Brown et al., 2013). Finally, Also an important advantage
537 of ORCHIDEE is that it includes the last century change in crop production calibrated against data (Guenet et al., 2018).

538
539 For the validation of the spatial variability of the SOC stocks of hillslopes and floodplains we used the scaling relationships
540 between basin area and SOC storage derived by Hoffmann et al. (2013a). The study by Naipal et al. (2016) found that the
541 global sediment budget model is able to reproduce the scaling behaviour of parameters for sediment storage, and a
542 analyzing the dependence of this scaling behavior on the main parameters of the model, they argue that the scaling is an
543 emergent feature of the model and mainly dependent on the underlying topography. This indicates that the scaling features
544 of floodplain and hillslope sediment and C storage should also be applicable to a the more recent time period, such as in
545 our study. In order In our study we aim to evaluate the ability of CE-DYNAM to reproduce this scaling behavior for the
546 SOC storage, of the Rhine. For this purpose we selected the grid cells that contained the points of observation of the study
547 of Hoffmann et al. (2013a) and performed a regression of the basin area (defined as the upstream contributing area) and the
548 SOC storage of that gridcell for floodplains and hillslopes separately. Comparing the absolute values of the sediment and
549 SOC storages of each grid cell from Hoffmann et al. (2013a) was not possible due to the difference in the time-period of
550 the studies, where Hoffmann et al. (2013a) focussed on the entire Holocene, while our study focussed only on the period
551 from 1850 AD.

552
553 For the validation of the total SOC stocks we used the Global Dataset for Earth System Modeling (GSDE) (Shangguan et
554 al., 2014) available at a spatial resolution of 1km and the Land Use/Land Cover Area Frame Survey (LUCAS) (Palmieri et

555 al., 2011). The LUCAS topsoil SOC stocks, available at a high spatial resolution of 500 m, were calculated using the
556 LUCAS SOC content for Europe (de Brogniez et al., 2015) and soil bulk density derived from soil texture datasets
557 (Ballabio et al., 2016).

558

559 **3 Results**

560

561 Due to large uncertainties in the model and validation data for the Alpine region we only present and discuss the model and
562 validation results for the non-Alpine part of the Rhine catchment.

563

564 **3.1 Model validation**

565 In this section we present the model validation results using the methods and ~~validation~~ data described in detail in the
566 previous section.

567

568 We find that the quantile distribution of the simulated gross soil erosion rates compares well to the distributions of other
569 observational and high-resolution modelling studies (Cerdan et al., 2010, Panagos et al., 2015, Bug et al., 2014), ~~although~~
570 ~~CE-DYNAM usually underestimates the very large soil erosion rates such as is found by Cerdan et al. (2010)~~ (Fig 3A, B,
571 C). ~~This is due to the coarse spatial and temporal resolution of CE-DYNAM, and the lack of the slope-length factor (L)~~
572 ~~(Cerdan et al. (2010) assumed a constant slope length of a 100m).~~ It should be noted that our study, ~~the study of~~ Cerdan et
573 al. (2010) and Bug et al. (2014) simulated potential soil erosion rates, not accounting for erosion control practices
574 ~~represented that are captured~~ by the P-factor.

575

576 We also find that the quantile distribution of the simulated net soil erosion from hillslopes in our study compares well with
577 the distribution from the high-resolution modelling study of Borrelli et al. (2018) (Fig 3D). ~~In addition~~ ~~Furthermore~~, we
578 performed a spatial comparison of our simulated gross and net erosion rates to those of the studies mentioned above. For
579 this purpose we delineated 13 sub-basins in the Rhine catchment (Fig S3). Table 3 summarizes the resulting goodness-of-fit
580 statistics of this comparison and shows that our erosion model is generally in good agreement with the other studies at
581 sub-basin level, ~~except for net soil erosion. The estimation of the net soil erosion between our study and the study of~~
582 ~~Borrelli et al. (2018) is done in different ways, which may explain the difference in the results. In our study the deposition~~
583 ~~of sediment in hillslopes is explicitly calculated as a function of the slope, and vegetation type/cover. Borrelli et al. (2018)~~
584 ~~used the transport capacity concept (Van Rompaey et al., 2001). Both methods have their uncertainties when applied at~~
585 ~~large spatial scales. The method in our study has been designed and calibrated to be used at a large spatial scale, and at~~
586 ~~coarse resolution, while the method of Borrelli et al. (2018) was originally designed to be applied at spatial scales <100m.~~

587

588 We find that the quantile distributions of our simulated agricultural ~~Carbon~~ erosion and deposition rates are similar to
589 those of the high-resolution modelling study of Lugato et al. (2018) (Fig 4A-D). Also the spatial variability of the C

590 erosion rates at sub-basin level is in good comparison to the validation data (Table 4). However, the linear regression
591 between soil erosion and C erosion rates of our study lies at the lower end of the relationships derived from the enhanced
592 and reduced erosion scenarios of Lugato et al. (2018) (Fig 5). ~~On the one hand, our study does not include erosion-control~~
593 ~~(EC) practices, leading to substantially larger simulated soil erosion rates in regions with EC. Figure 5 shows that our~~
594 ~~simulated erosion rates are in general larger than the erosion rates from Lugato et al. (2018), which may be explained by~~
595 ~~this mechanism. On the other hand, the C erosion rates of our study are lower than those of Lugato et al. (2018), due to the~~
596 ~~coarse spatial resolution of our underlying C-scheme derived from the ORCHIDEE LSM. This could be explained by the~~
597 ~~fact that we do not explicitly consider erosion-control and management practices on agricultural land, and the coarse~~
598 ~~resolution of our model.~~ The decreased spread in our simulated values is also a result of the coarse resolution of our
599 model.

600
601 Accounting for erosion, deposition and transport of SOC leads to a better representation of the simulated topsoil C stocks
602 per land cover type when compared to SOC stocks of the LUCAS database (Fig 6). The simulated SOC stocks of the top
603 20 cm of the soil profile fall within the quantile range of the LUCAS SOC stocks for cropland and forest (Fig 6). ~~Although~~
604 ~~the topsoil SOC stocks for grassland improved but still show a large uncertainty range remains.~~ Furthermore, we find that
605 in both the erosion and no-erosion simulation the SOC stocks for grassland are higher than for forest. This is also observed
606 in the study of Wiesmeier et al. (2012), ~~in South-Germany~~ where they found considerable higher SOC stocks for grassland
607 with a median of 11.8 kg C m⁻² compared to forest based on the analysis of 1460 soil profiles ~~in South-Germany~~.
608 Furthermore, the comparison of the simulated total SOC stocks to those of the LUCAS and GSDE databases at sub-basin
609 level shows a good model performance with respect to the spatial variability in topsoil SOC stocks (Table 5). To validate
610 the spatial variability of floodplain and hillslope SOC stocks separately, we used the scaling relationships found by
611 Hoffmann et al. (2013a) (section 2.12). We find a significantly larger exponent for the scaling relationship between the
612 simulated floodplain SOC storage and basin area compared to the simulated hillslope SOC storage, when using the grid
613 cells that contain the points of observation corresponding to the study of Hoffmann et al. (2013a). This result is in line with
614 what Hoffmann et al. (2013a) found and shows that CE-DYNAM can realistically reproduce the spatial variability in SOC
615 stocks between hillslopes and floodplains (Table 6). However, when deriving the scaling relationships at sub-basin level
616 instead of using individual grid cells we do not find a significant difference in scaling between floodplains and hillslopes
617 (Table 6).

618 619 **3.2 Model application**

620
621 We find an average annual soil erosion rate of 1.44±0.82 t ha⁻¹ year⁻¹ over the period 1850-2005, which is about half of the
622 average erosion rate simulated for the last millennium (Naipal et al., 2016) and falls ~~within~~ into the range of the average
623 erosion rates of the Holocene (Hoffmann et al., 2013). This soil erosion flux mobilized around 66±28 Tg of C over the

624 same time period ~~1850-2005~~, of which on average ~~about~~ 57% is deposited in colluvial reservoirs, 43% is deposited in
625 alluvial reservoirs, and ~~while~~ 0.2% is exported out of the catchment.

626
627 The lower average annual soil erosion rate over the study period compared to the last millennium is a result of the general
628 afforestation in the non-Alpine part of the Rhine catchment that started around 1910 AD (~~Fig 7B~~) according to the data on
629 land cover and land use (Peng et al., 2017; Fig 7B). This ~~land cover data~~ also shows that forest increases by 24% over the
630 period 1910-2005, mostly as a result of grassland to forest conversion. Cropland decreases by 6% over the period 1920 and
631 1970, and is relatively stable afterwards. This afforestation leads to a long-term decreasing trend in gross soil and SOC
632 erosion rates on hillslopes (Fig 7C). The temporal variability in the soil and C erosion rates is a result of direct changes in
633 precipitation, such as the temporary increase in erosion rates over the period 1940-1960 (Fig 7A). Furthermore, we find
634 that the temporal variability in C erosion rates follows the soil erosion rates closely, indicating that soil erosion dominates
635 the variations in C erosion over this time-period, while increased SOC stocks due to CO₂ fertilization and afforestation play
636 a secondary role as a slowly varying trend. It should be noted that the correlation between soil and C erosion might be
637 affected by processes not properly captured by the model such as the selectivity of erosion including ~~, which also include~~
638 the enrichment of C in eroded material.

639
640 The cumulative C erosion removal flux of 66±28 Tg of C leads to a cumulative net C sink for the whole Rhine region of
641 216±23 Tg C (Fig 7D). This is about 2.1 – 2.7 % of the cumulative NPP and of the same magnitude as the cumulative land
642 C sink of the Rhine without erosion. It should be noted that these are potential fluxes, assuming that the photosynthetic
643 replacement of C is not affected by the degradation of soil due to the removal of nutrients, declining water-holding capacity
644 and other negative changes to the soil structure and texture (processes not covered by our model). The breaking point in
645 figure 7D around 1910 AD is a result of the climate data used as input.

646
647 To better understand the erosion-induced net C flux, we analyze the erosion-induced C exchange with the atmosphere by
648 creating C budgets for the entire Rhine catchment for the period 1850-1860 and for the period 1950-2005 (Fig 8A&B).
649 These C budgets also shed light on changes in the linkage between lateral and vertical C fluxes over time. As we do not
650 explicitly track the movement of eroded C through all reservoirs (for example between eroding hillslopes and colluvial
651 reservoirs), we make use of the changes in SOC stocks and ~~NEP~~ Net Ecosystem Productivity (NEP), which is the
652 difference between NPP and heterotrophic respiration, of the three main simulations (S0, S1, S2) to derive the
653 erosion-induced vertical C fluxes. By subtracting the ~~NEP~~ Net Ecosystem Productivity of hillslopes (NEP_{HS}); which is the
654 difference between NPP and heterotrophic respiration, of the no-erosion simulation (S0) from the erosion-only simulation
655 (S1), we derive the additional photosynthetic replacement of SOC on eroding sites (Eq. 21):

656
657
$$E_{rep} = NEP_{HS}(S1) - NEP_{HS}(S0) \tag{21}$$

658

659 Where, E_{rep} is the potential dynamic Photosynthetic replacement of C on eroding sites (assuming no feedback of erosion on
660 NPP). Part of the eroded C that is transported to and deposited in colluvial reservoirs can be respired or buried (Eq. 22).
661 The difference between NEP of simulation S2 and S1 is the NEP caused by the deposition of eroded C in colluvial areas
662 and equal to the difference between the burial and respiration of C in colluvial sites. As we do not explicitly track the
663 respiration of deposited material in the model, we can only derive the net respiration or net burial of colluvial deposits
664 ($R_{C_{net}}$) with the following equation:

$$665 \\ 666 R_{C_{net}} = NEP_{HS}(S2) - NEP_{HS}(S1) \quad (22)$$

667
668 The same concept can be applied for the net respiration of floodplains:

$$669 \\ 670 R_{a_{net}} = NEP_{FL}(S2) - NEP_{FL}(S0) \quad (23)$$

671
672 Where, NEP_{FL} is the floodplain ~~NEP-Net Ecosystem Productivity~~, and $R_{a_{net}}$ is the net respiration or net burial of alluvial
673 deposits. Positive values for $R_{a_{net}}$ or $R_{C_{net}}$ indicate a net burial (respiration S2 < respiration S0/S1) of the deposited
674 material.

675
676 We find that the dynamic replacement of C on eroding sites increased by 17-33% at the end of the period despite
677 decreasing soil erosion rates (Figs 8A & B). This increase in the photosynthetic replacement of C is due to the globally
678 increasing CO₂ concentrations that lead to the CO₂ fertilization effect, amplified by the afforestation trend in the Rhine over
679 this period. Without this fertilization effect, soil erosion and deposition would be likely a weaker C sink or even a C source
680 over the period 1850-2005 (Figs S4-A & B). This CO₂ fertilization effect promotes a 100 % replacement of the eroded C on
681 hillslopes and even leads to a C sink on hillslopes at the end of the study period (Fig 8B). Furthermore, we find that the
682 yearly average gross C erosion flux from eroding sites decreases by 10 - 34 %, while the yearly deposition fluxes in
683 colluvial and alluvial sites decreases by 20 % and 19 - 47 %, respectively. The decrease in the deposition flux to
684 floodplains is compensated by a better sediment connectivity between hillslopes and floodplains due to afforestation.
685 Forests have less man-made structures that can prevent the erosion fluxes from reaching the floodplains, which is
686 represented by a higher floodplain deposition ' f ' factor in the model. The decrease in the erosion flux also leads to a
687 decreased POC export of the catchment at the end of the study period.

688
689 We also find that both the colluvial and alluvial reservoirs show a net respiration flux throughout the time period (Figs 8A
690 & B). This is consistent with previous studies who found that deposition sites can be areas of increased CO₂ emissions
691 (Billings et al., 2019; Van Oost et al., 2012). However, there is a slight difference in the respiration of deposited C between
692 the start and end of the transient period. The respiration of deposited SOC in colluvial sites increases with time while the
693 respiration of deposited SOC in alluvial sites shows rather a decreasing trend. These changes in SOC respiration of

694 deposited material depends on (1) the amount of deposited material, (2) increasing temperatures over 1850-2005 for the
695 entire catchment, and (3) the constant removal of C-rich topsoil and its deposition in alluvial and colluvial reservoirs,
696 which makes the deposited sediments generally richer in C than soils on erosion-neutral sites, providing more substrate for
697 respiration. The largest increase in total respiration of alluvial and colluvial deposits takes place in hilly regions due to the
698 initial increase in erosion rates resulting in large deposits of C. Overall, we find that the increased respiration of deposited
699 material slightly offsets the increased dynamic C replacement, however, the dynamic C replacement on eroding sites still
700 dominates the erosion-induced C sink.

701

702 **4 Discussion**

703

704 In this ~~section~~chapter we discuss some of the most important model limitations, uncertainties and assumptions.

705

706 **4.1 Initial conditions and past global changes**

707

708 Initial climate and land cover/use conditions, ~~needed to perform the equilibrium simulation together with~~ and the length of
709 the transient period are essential parameters that determine the resulting spatial distribution of soil and C. Landscapes are
710 in a constant transient state due to global changes, such as climate change, land use change, accelerated soil erosion.
711 However, we assumed an equilibrium state so that we can quantify the changes during the transient period. ~~The more one~~
712 ~~goes back in time to select the initial conditions and the~~ longer the transient period that covers the essential historical
713 environmental changes, the more accurate are the present-day distribution of SOC stocks, sediment storages, and related
714 fluxes. This is especially true when analyzing the redistribution of soil and C as a result of erosion, deposition and
715 transport, as these soil processes can be very slow. For example, the study of Naipal et al. (2016) showed that by
716 simulating the soil erosion processes for the last millennium a spatial distribution of sediment storages that is similar to
717 observations can be found. In this study we ~~simulated~~modeled the steady state based on the initial conditions of the period
718 1850-1860 due to constraints in data availability on precipitation and temperature, ~~and because the aim of this study is to~~
719 ~~present the potential and limitations of the new model CE-DYNAM rather than provide precise values for soil storages,~~
720 ~~and C stocks and fluxes.~~ By focusing only on the period 1850-2005 we miss the effects of significant land use changes in
721 the past that coincided with times of strong precipitation such as in the 14th and 18th century (Bork et al., 2003). These
722 major anthropogenic changes in the last Holocene substantially affected the present-day spatial distribution and size of
723 sediment storage and SOC stocks.

724

725 The absolute value of the SOC storage from the S2 simulations of the non-Alpine region of the Rhine catchment for the
726 year 2005 is in the range of 2.74-2.99 Pg of C, which is larger than the 1.7±0.6 Pg of C that Hoffmann et al. (2013a)
727 measured. It should be noted that the ORCHIDEE model (S0 simulation) already overestimates the total SOC stock of the
728 non-Alpine region of the Rhine (2.43 Pg of C), when the initial conditions of the period 1850-1860 are used. Due to the

729 fact that we miss the climate and land use changes before the year 1850, we find that floodplains store less SOC than
730 hillslopes. Although this is in contrast to the findings of Hoffmann et al. (2013a), the difference in SOC stocks between
731 floodplains and hillslopes from the S2 simulations is better than the difference derived from the S0 simulation. We find that
732 floodplains store 1.28-1.72 and hillslopes 1.7-2 Pg of C when erosion and deposition processes are taken into account,
733 compared to 0.69 Pg of C for floodplains and 2.29 Pg of C for hillslopes when these processes are lacking.

734
735 ~~As a result, our model shows that floodplains store less SOC than hillslopes. However, We do also~~ find that floodplains
736 have an overall higher C concentration (12 kg m^{-2}) compared to hillslopes (9 kg m^{-2}) at the end of the transient period (Fig
737 9A), which is in line with the findings of Hoffmann et al. (2013a) and what can be derived from global soil databases. This
738 is a result of higher SOC concentrations in deeper soil layers of floodplains compared to hillslopes (Fig 9 A & B), ~~=~~
739 ~~Although, the difference in C concentrations between floodplains and hillslopes is not as significant as is also shown in the~~
740 ~~study of Hoffman et al. (2013). To be closer to the observational difference between floodplains and hillslopes we would~~
741 ~~need to consider the period before 1850, extreme climate events, and a higher plant productivity in floodplains resulting~~
742 ~~from favorable soil nutrient and hydrological conditions. This is due to the absence of a higher local plant productivity~~
743 ~~resulting from favorable soil nutrient and hydrological conditions in our modelled floodplains.~~

744

745 **4.2 Model advantages and limitations**

746

747 Although we parameterized and applied CE-DYNAM for the Rhine catchment, it is intended to be made applicable to
748 other large catchments ~~globally~~. CE-DYNAM combines soil erosion processes, for which small scale differences in
749 topography are of utter importance, with a state-of-the-art representation of large-scale SOC dynamics driven by land use
750 and environmental factors (climate, atmospheric CO_2) as simulated by the ORCHIDEE LSM. The flexible structure of
751 CE-DYNAM makes the model adaptable to the SOC dynamics of other LSMs. In this way it is possible to study the main
752 processes behind the linkages between soil erosion and the global C cycle.

753

754 CE-DYNAM explicitly accounts for hillslope and floodplains re-deposition, which is to our knowledge unique for a
755 large-scale C erosion model and highly novel. However, it still lacks important processes affecting the C dynamics in
756 floodplains. The model does not account for a slower respiration rate due to low-oxygen conditions, physical and chemical
757 stabilization (Berhe et al., 2008; Martínez-mena et al., 2019) or a higher NPP for nutrient-rich floodplains (Van Oost et al.,
758 2012; Hoffmann et al., 2013). The oxidation and preservation of C in deposition environments, especially in alluvial
759 reservoirs remain highly uncertain (Billings et al., 2019).

760

761 Due to its simplistic nature and coarse-resolution, CE-DYNAM does not resolve rivers and streams explicitly but assumes
762 that they are included in the floodplain parts of the grid cells. ~~As a result, CE-DYNAM does not differentiate between~~
763 ~~eroded hillslope soil that reaches the water network directly (where the residence time of suspended sediment is in the~~

764 order of days), and the sediment that is first retained in the floodplains before it reaches the water network due to fluvial
765 erosion (sediment residence time is in the order of a few to thousands of years). CE-DYNAM has been developed and
766 calibrated to simulate long-term changes in sediment and C storage on land and not the short-term variations in sediment
767 and POC fluxes carried by rivers. This limits the application of CE-DYNAM in its current form to accurately quantify
768 sediment and POC fluxes of rivers and streams, and to compare them to observations.

769
770 CE-DYNAM produces a sediment export flux at the end of the year 2005 of about 64721.6×10^7 tonnes per year, which is
771 about two orders of magnitude lower than the estimated measured suspended sediment flux of about 3.15×10^6 tonnes
772 per year from (Asselman et al. (2003) or the 0.75×10^6 tons year⁻¹ simulated by Li et al. (2020). This sediment export rate
773 leads to a yearly sediment bound POC export of about 2×10^8 g C year⁻¹ 2005. This POC flux is also two orders of
774 magnitude lower than the 2.6×10^{10} g C year⁻¹ given by the GlobalNEWS2 model (Mayorga et al., 2010) or the 1.5×10^{11} g C
775 year⁻¹ found by Beusen et al. (2005), which is mainly a result of the underestimated simulated sediment export rate.

776
777 Furthermore, CE-DYNAM does not simulate fluvial erosion as a complex function of the channel geometry, riverbank
778 erodibility and sheer stress (Dröge et al., 1992), due to the lack of data on these parameters at the regional scale, and to
779 keep a balance between model complexity and its computational ability. Also, our model does not resolve erosion of the
780 deposited river sediment by flooding events. This simplified model concept for fluvial erosion contributes to the
781 underestimation of sediment and C export in floodplains. Finally, with the current model setup we do not account for large
782 soil erosion events before 1850 or extreme precipitation events that may have a long-term effect on the sediment export
783 rate of the Rhine.

784
785 Although we underestimate the riverine sediment and POC fluxes, we find that the spatial variability in sediment storage
786 and SOC stocks of the sub-basins are within or close to observational uncertainty ranges (Table 5, 6; Naipal et al., 2016).
787 We also find that the C density in the topsoil layers of floodplain soils located downstream of the Rhine and the C
788 concentration of the POC flux are realistic. We find a C concentration of ~3.3% in the exported fine sediments. Abril et al.
789 (2005) found a 5.5% POC mass fraction in suspended sediments for the Rhine. The C density of the topsoil layer of the
790 floodplains in the downstream grid cells in the S2 simulations (S2, S2_min, S2_max) is on average 4.47 kg C m^{-2} , which
791 falls within the range of the average C density of $5.13 \pm 1.3 \text{ kg C m}^{-2}$ measured by Hoffmann et al. (2013a) for floodplain
792 overbank deposits. By comparison, the average C density of the topsoil layers of downstream grid cells in the S0
793 simulation is $12.78 \text{ kg C m}^{-2}$, which is an overestimation. Other model uncertainties that may affect the SOC stocks and
794 POC fluxes include: (1) The absence of increased plant productivity of floodplains, and transformations between POC,
795 DOC and CO₂, and their fate in rivers and streams. Increased plant productivity of floodplains is shown to contribute
796 significantly to the higher SOC stocks of floodplains compared to hillslopes, and to the export of DOC and POC to rivers
797 (Van Oost et al., 2012; Hoffmann et al., 2013a).

798

799 In a future study we aim to improve the sediment and POC export, and account for a higher floodplain plant productivity
800 by using a nutrient-enabled version of the ORCHIDEE LSM (Goll et al., 2017).

801 ~~The higher sediment flux is the result of absent riverine processes in CE-DYNAM such as river embankment, sediment~~
802 ~~burial behind dams, and the fact that we assume an equilibrium state for the Rhine catchment based on the period~~
803 ~~1850-1860 where agricultural soil erosion rates were already high. The simulated total cumulative sediment export of 2.5~~
804 ~~Gt for the Rhine over the period 1850-2005 is about 36 % of the cumulative gross soil erosion flux of 6.8 Gt. This sediment~~
805 ~~flux leads to a cumulative POC export of about 0.14 Tg of C for the Rhine over the period 1850-2005. This is 0.2 % of the~~
806 ~~cumulative C erosion flux. The yearly POC flux at the end of the year 2005 is 0.02 tC km² year⁻¹ (normalized over the~~
807 ~~total basin area), which is an order of magnitude lower compared to other studies who found a total POC export for the~~
808 ~~Rhine of about 0.9 t C km² year⁻¹ (Beusen et al., 2005; Sorribas et al., 2017). This underestimation in POC in~~
809 ~~CE-DYNAM is most likely a result of the high sediment residence time of floodplains downstream of the Rhine and the~~
810 ~~absence of increased plant productivity of floodplains, leading to the decomposition of a large fraction of the deposited C.~~
811 ~~Increased plant productivity of floodplains is shown to contribute significantly to the higher SOC stocks of floodplains~~
812 ~~compared to hillslopes, and to the export of DOC and POC to rivers (Van Oost et al., 2012; Hoffmann et al., 2013). In~~
813 ~~addition, the model lacks processes that account for the transformations between POC, DOC and CO₂ and their fate in~~
814 ~~rivers and streams. The model also assumes a ‘natural’ state of the catchment where there is no river embankment and the~~
815 ~~floodplains are more or less dynamic. This may affect the behaviour of the POC export and residence time of C in~~
816 ~~floodplains.~~

817
818 Furthermore, the model does not take into account the full effects of the selectivity of erosion, often expressed as the
819 enrichment ratio, where the C content of eroding soil or the deposited sediment can be different from that of the original
820 soil. The enrichment ratio ~~varies substantially~~ can be very variable across landscapes, while the importance of erosion
821 selectivity for C is still under debate (Nadeu et al., 2015; Wang et al., 2010). However, we did a simple sensitivity test to
822 study the effect of C enrichment by erosion (section 4.3).

823
824 CE-DYNAM does not account for different ratios between the SOC pools (active, slow, passive) with depth due to the
825 limitation in information to constrain these fractions for floodplains and hillslopes. However, this can be potentially
826 important for respiration of C in depositional sites and during transport. Studies show that the labile C is decomposed first
827 during sediment transport and directly after deposition, leaving behind the more recalcitrant C in deposition sites (Berhe et
828 al., 2007; Billings et al., 2019). Due to the simplistic nature of our coarse-resolution model and the lack of data on
829 oxidation of eroded C during transport we did not include C respiration during transport in the model.

830
831 The current SOC scheme of CE-DYNAM does also not account for different residence times of SOC as a function of
832 landscape position along a hillslope. The SOC decomposition rates can vary significantly along a hillslope due to changes
833 in soil moisture, temperature, aggregation, and the transport of minerals and nutrients (Doetterl et al., 2016). Currently,

834 these processes are not resolved in coarse resolution LSMs, contributing to the uncertainty in the large-scale linkage
835 between soil erosion and SOC dynamics.

836
837 Furthermore, there is no feedback between soil erosion and plant productivity in the model. To account for ~~this feedback~~
838 ~~such process~~ soil erosion processes would need to be explicitly included in an LSM, such as ORCHIDEE, which would
839 increase the computational complexity of the simulations substantially. The lack of this feedback results in an unlimited
840 dynamic replacement of C on eroding sites.

841
842 Currently, the erosion ~~schememodule~~ of CE-DYNAM does not include the L (slope-length) and P (support-practice)
843 factors. This might induce some bias in the results, especially for agricultural land. In a ~~future~~ ~~our next~~ study we aim to
844 make CE-DYNAM better applicable for agricultural land, where these factors play an important role. For this purpose we
845 will focus on the development of new methods that can quantify the L and P factors reliably at the global scale, and will
846 need to re-calibrate ~~the erosion scheme module of CE-DYNAM,~~ the Adj.RUSLE. Our decision of leaving out the L and P
847 factors from the erosion equation in our study is based on the global study of Doetterl et al. (2012), which showed that the
848 S, R, C and K factors explain approximately 78 % of the total erosion rates on cropland in the USA. This indicates that on
849 cropland the L and P factors, which are related to agriculture and land management, contribute only for 22 % to the overall
850 erosion rates. This percentage is comparable to the uncertainty range in the estimation of the S, R, C and K factors at the
851 regional scale from coarse resolution data. Renard and Ferreira (1993) also mention that the soil loss estimates are less
852 sensitive to slope length than to most other factors. Furthermore, various studies argue that the estimation of the L factor
853 for large areas is complicated and thus can induce significant uncertainty in soil erosion rates calculated based on coarse
854 resolution data (Foster et al., 2002; Kinnell, 2007). Especially, for natural landscapes, such as forest, the estimation of the
855 L factor is not straightforward as these natural landscapes usually include steep slopes (Elliot, 2004). In order to stay
856 consistent with the estimation of potential soil erosion for all land cover types, we removed the L factor from the equation.
857 The Adj.RUSLE has been already successfully validated at the regional scale, without the L and P factors where the spatial
858 variability of soil erosion rates compares well to other high resolution modeling studies and observational data and the
859 absolute values fall within the uncertainty ranges of those validation data (Naipal et al., 2015; Naipal et al., 2016; Naipal et
860 al., 2018; and this study). Finally, the aim of this study was to develop and validate a ~~Carbon~~ ~~erosion scheme module~~ for
861 applications at the global scale, where the estimation of the L and P factors is ~~even~~ more limited. By showing that the
862 erosion rates from the Adj.RUSLE and CE-DYNAM are within the uncertainty of other data and modelling studies, we ~~can~~
863 assume that it will be applicable for other large catchments in the temperate region.

864
865 Finally, CE-DYNAM considers only the rather 'slow' rill and interrill soil erosion processes, and does not take into
866 account ~~severe erosion processes such as~~ gully erosion and landslides, which are bound to extreme precipitation events.
867 The daily timestep of CE-DYNAM and the current setup of the sediment budget module allows only for long-term yearly
868 average changes in erosion and deposition rates and cannot be applied to estimate episodic erosion and deposition events.

869

870 4.3 Sensitivity analysis

871

872 We analyzed the effects of the following model assumptions: (1) C enrichment during erosion, (2) the floodplain sediment
873 residence time, and (3) crop residue management.

874

875 To test the C enrichment we increased the EF (Eq. 15) from 1 to 2, assuming a strong enrichment of C during erosion
876 (section 2.11). We find that this enrichment results in a gross C erosion flux that is 1.61 times larger than compared to the
877 flux without enrichment (Table 7). This leads also to a larger dynamic replacement of C on eroding sites in combination
878 with a larger burial in depositional sites, which is in accordance with the study of Lugato et al. (2018). The resulting C sink
879 from the enrichment simulation is 1.25 times larger than the sink under default conditions. However, we do not find a
880 significant effect on the cumulative POC export flux under C enrichment (Table 7).

881

882 To test the potential effects of a different sediment residence time on the SOC dynamics, we performed a sensitivity study
883 where we changed the basin average sediment residence time to be 50% higher or 50% lower but keeping the maximum
884 sediment residence time at 1500 years (section 2.11). By changing the average sediment residence time and keeping the
885 maximum fixed, it will be the grid cells with the lowest residence times that will undergo the largest changes in the
886 residence time and consequently in the floodplain SOC storage and export. The higher the residence time, the longer the
887 deposited soil C will reside in the floodplains, where it can either be respired or buried in deeper soil layers. Therefore, we
888 find that the effects of the sediment residence time on the SOC dynamics are non-linear. Under default conditions we find
889 the highest SOC storage. A 50 % higher average sediment residence time leads to the lowest total SOC storage, with a
890 decrease of 30 % compared to default conditions, while the erosional C sink is reduced by 20 % (Table 7). This could be
891 explained by a higher C decomposition flux for floodplains due to the long residence time of C in deposition areas.
892 Especially in mountainous regions where the soil erosion flux is large and removes a large part of the labile C, a higher
893 sediment residence time will lead to higher C decomposition emissions due to decomposition in floodplains. The turnover
894 seems to dominate over the C burial in deeper layers and export. A 50 % lower average sediment residence time also leads
895 to a decrease (of 8 %) in the total SOC storage and a decrease of 6 % in the erosional C sink compared to default
896 conditions (Table 7). Also here, the largest changes are found in mountainous regions where a low sediment residence time
897 leads to a large export of C, which is then deposited in lower lying, more extensive floodplains. Thus, increasing or
898 decreasing the residence time leads to a smaller total SOC storage, resulting from different spatial distributions of this SOC
899 storage. The POC flux under the highlow sediment residence time scenario is substantially higher than under default
900 conditions (Table 7).

901

902 To test the effects of crop residue management we harvested all above-ground crop residues (section 2.11). We find that the
903 total litter C stock is about 15 % smaller than compared to the default case by the end of the year 2005. This leads to a
904 total change in the transient SOC stocks that is 20 % smaller under no erosion (S0), and 26 % smaller under erosion (S2)

905 (Table 7). Our findings confirm that soil management practices such as residue management have a substantial effect on the
906 SOC dynamics.

907

908 **5 Conclusions**

909

910 We presented a novel spatially-explicit and process-based C erosion dynamics model, CE-DYNAM, which simulates the
911 redistribution of soil and C over land as a result of water erosion and ~~estimates the implications~~ ~~calculates the role of this~~
912 ~~redistribution~~ for C budgets at catchment scale. We demonstrated that CE-DYNAM captures the spatial variability in soil
913 erosion, C erosion and SOC stocks of the non-Alpine region of the Rhine catchment when compared to high-resolution
914 estimates and observations. We also showed that the quantile ranges of erosion and deposition rates and C stocks fall
915 within the uncertainty ranges of previous estimates at basin or sub-basin level. Furthermore, we demonstrated the model
916 ability to disentangle vertical C fluxes resulting from the redistribution of C over land and develop C budgets that ~~can~~ shed
917 light on the role of erosion in the C cycle. The simple structure of CE-DYNAM and the relative low amount of parameters
918 make it possible to run several simulations to investigate the role of individual processes on the C cycle such as removal by
919 erosion only, or the role of deposition and transport. Its compatibility with land surface models makes it possible to
920 investigate the long-term and large-scale effect of erosion processes under various global changes such as increasing
921 atmospheric CO₂ concentrations, changes to precipitation and temperature, and land use change.

922

923 The application of CE-DYNAM for the Rhine catchment for the period 1850-2005 AD reveals three key findings:

- 924 ● Soil erosion leads to a cumulative net C sink of 216±23 Tg by the end of the period, which is in the same order of
925 magnitude as the cumulative land C sink of the Rhine without erosion. This C sink is a result of an increasing
926 dynamic replacement of C on eroding sites due to the CO₂ fertilization effect, despite decreasing soil and C
927 erosion rates over the largest part of the catchment. We conclude that it is important to take **into account** global
928 changes such as climate change ~~in order into account~~ to better quantify the net effect of erosion on the C cycle.
- 929 ● After performing a sensitivity analysis on key model parameters we find that the C enrichment by erosion, crop
930 residue management and ~~a different spatial variability of~~ the residence time of floodplain sediment can
931 substantially change the overall values of C fluxes and SOC storages. However, the main findings, such as soil
932 erosion being a net C sink for the Rhine catchment, remain.
- 933 ● Initial climate and land cover conditions and the transient period over which erosion under global changes takes
934 place are essential for ~~determining the determination~~ if soil erosion is a net C sink or source and to what extent.

935

936 Altogether, these results indicate that despite model uncertainties related to the relative coarse spatial resolution, missing or
937 simplified processes, CE-DYNAM represents an important step forwards into integrating soil erosion processes and
938 sediment dynamics in Earth system models. The next step would be to improve CE-DYNAM with respect to riverine
939 sediment and POC export fluxes and management practices.

940

941 **Code and data availability**

942

943 The source code of CE-DYNAM is included as a supplement to this paper. Model data can be accessed from the Zenodo
944 repository under the doi:10.5281/zenodo.2642452 (not published yet). For the other data sets that are listed in Table 1, it is
945 encouraged to contact the first authors of the original references.

946

947 **Author contributions**

948

949 VN built and implemented the mode. YW provided the basic structure for the model. All authors contributed in the
950 interpretation of the results and wrote the paper.

951

952 **Competing interests**

953

954 *The authors declare that they have no conflict of interest.*

955

956 **Acknowledgements**

957

958 Funding was provided by the Laboratory for Sciences of Climate and Environment (LSCE), CEA, CNRS, and UVSQ.
959 Victoria Naipal, Ronny Lauerwald and Philippe Ciais acknowledges support from the VERIFY project that received
960 funding from the European Union's Horizon 2020 research and innovation program under grant agreement No 776810.
961 Bertrand Guenet acknowledges support from the project ERANETMED2-72-209 ASSESS. We also thank Dr. S. Peng for
962 sharing the PFT maps.

963

964 **References**

965

966 [Abril, G. and Borges, A.V.: Carbon dioxide and methane emissions from estuaries, Greenhouse gas emissions—fluxes and
967 processes, 187-207, Springer, Berlin, Heidelberg, 2005.](#)

968

969 Asselman, N. E. M.: Suspended sediment dynamics in a large drainage basin : the River Rhine , 1450(November 1998),
970 1437–1450, [https://doi.org/10.1002/\(SICI\)1099-1085\(199907\)13:10<1437::AID-HYP821>3.0.CO;2-J](https://doi.org/10.1002/(SICI)1099-1085(199907)13:10<1437::AID-HYP821>3.0.CO;2-J) ,1999.

971

972 Asselman, N. E. M., Middelkoop, H. and van Dijk, P. M.: The impact of changes in climate and land use on soil erosion,
973 transport and deposition of suspended sediment in the River Rhine, Hydrol. Process., 17(16), 3225–3244,
974 doi:10.1002/hyp.1384, 2003.

975

976 Ballabio, C., Panagos, P. and Monatanarella, L.: Geoderma Mapping topsoil physical properties at European scale using the
977 LUCAS database, *Geoderma*, 261, 110–123, doi:10.1016/j.geoderma.2015.07.006, 2016.
978

979 Berhe, A. A., Harte, J., Harden, J. W. and Torn, M. S.: The Significance of the Erosion-induced Terrestrial Carbon Sink,
980 *Bioscience*, 57(4), 337, doi:10.1641/B570408, 2007.
981

982 Berhe, A. A., Harden, J. W., Torn, M. S. and Harte, J.: Linking soil organic matter dynamics and erosion-induced terrestrial
983 carbon sequestration at different landform positions, *J. Geophys. Res. Biogeosciences*, 113(4), 1–12,
984 doi:10.1029/2008JG000751, 2008.
985

986 Beusen, A. H. W., Dekkers, A. L. M., Bouwman, A. F., Ludwig, W., & Harrison, J.: Estimation of global river transport of
987 sediments and associated particulate C, N, and P, *Global Biogeochemical Cycles*, 19(4), doi:10.1029/2005GB002453,
988 2005.
989

990 Billings, S. A., Richter, D. D. B., Ziegler, S. E., Prestegard, K. and Wade, A. M.: Distinct Contributions of Eroding and
991 Depositional Profiles to Land-Atmosphere CO₂ Exchange in Two Contrasting Forests, 7(March),
992 doi:10.3389/feart.2019.00036, 2019.
993

994 [Bork, H.R. and Lang, A.: Quantification of past soil erosion and land use/land cover changes in Germany, Long term
995 hillslope and fluvial system modelling, 231-239, Springer, Berlin, Heidelberg, 2003.](#)
996

997 Borrelli, P., Van Oost, K., Meusburger, K., Alewell, C., Lugato, E., Panagos, P.: A step towards a holistic assessment of
998 soil degradation in Europe: Coupling on-site erosion with sediment transfer and carbon fluxes, *Environmental Research*,
999 161, 291-298, doi:https://doi.org/10.1016/j.envres.2017.11.009, 2018
1000

1001 de Brogniez, D., Ballabio, C., Stevens, A., Jones, R. J. A., Montanarella, L. and Van Wesemael, B.: A map of the topsoil
1002 organic carbon content of Europe generated by a generalized additive model, *Eur. J. Soil Sci.*, 66(January), 121–134,
1003 doi:10.1111/ejss.12193, 2015.
1004

1005 Bug, J., Stolz, W., Stegger, U.: Potentielle Erosionsgefaehrdung der Ackerboeden durch Wasser in Deutschland,
1006 Bundesanstalt fuer Geowissenschaften und Rohstoffe, www.bgr.bund.de/Boden, 2014
1007

1008 Cerdan, O., Govers, G., Le Bissonnais, Y., Van Oost, K., Poesen, J., Saby, N., Gobin, a., Vacca, a., Quinton, J.,
1009 Auerswald, K., Klik, a., Kwaad, F. J. P. M., Raclot, D., Ionita, I., Rejman, J., Rouseva, S., Muxart, T., Roxo, M. J. and
1010 Dostal, T.: Rates and spatial variations of soil erosion in Europe: A study based on erosion plot data, *Geomorphology*,
1011 122(1–2), 167–177, doi:10.1016/j.geomorph.2010.06.011, 2010.

1012
1013 Ciais, P., Sabine, C., Bala, G., Bopp, L., Brovkin, V., Canadell, J., Chhabra, A., DeFries, R., Galloway, J., Heimann, M.,
1014 Jones, C., Quéré, C. Le, Myneni, R. B., Piao, S. and Thornton, P.: Carbon and Other Biogeochemical Cycles, in Climate
1015 Change 2013: The physical science basis. Contribution of working group I to the fifth assessment report of the
1016 intergovernmental panel on climate change [Stocker, T.F., D. Qin, G.-K. Plattner, M. Tignor, S.K. Allen, J. Boschung, A.
1017 Nauels, Y. Xia, pp. 465–570, Cambridge University Press, Cambridge, United Kingdom and New York, NY., 2013.
1018
1019 De Moor, J. J. W., & Verstraeten, G.: Alluvial and colluvial sediment storage in the Geul River catchment (The
1020 Netherlands)—combining field and modelling data to construct a Late Holocene sediment budget, *Geomorphology*,
1021 95(3-4), 487-503, 2008
1022
1023 Doetterl, S., Van Oost, K. and Six, J.: Towards constraining the magnitude of global agricultural sediment and soil organic
1024 carbon fluxes, *Earth Surf. Process. Landforms*, doi:10.1002/esp.3198, 2012.
1025
1026 Doetterl, S., Berhe, A. A., Nadeu, E., Wang, Z., Sommer, M., & Fiener, P.: Erosion, deposition and soil carbon: a review of
1027 process-level controls, experimental tools and models to address C cycling in dynamic landscapes, *Earth-Science Reviews*,
1028 154, 102-122, 2016.
1029
1030 Dotterweich, M.: Geomorphology The history of human-induced soil erosion : Geomorphic legacies , early descriptions
1031 and research , and the development of soil conservation — A global synopsis, *Geomorphology*, 201(November), 1–34,
1032 doi:10.1016/j.geomorph.2013.07.021, 2013.
1033
1034 [Dröge, B., Engel, H., & Götz, E.: Channel erosion and erosion monitoring along the Rhine River, *Erosion and Sediment*](#)
1035 [Transport Monitoring Programmes in River Basins](#), 210, 493-503, 1992.
1036
1037 Elliot, W. J.: WEPP INTERNET INTERFACES FOR FOREST EROSION PREDICTION 1, *JAWRA Journal of the*
1038 *American Water Resources Association*, 40(2), 299-309, 2004.
1039
1040 Erkens, G.: Sediment dynamics in the Rhine catchment, Utrecht University, Faculty of Geosciences, Utrecht., 2009.
1041
1042 Foster, G. R., Yoder, D. C., Weesies, G. A., McCool, D. K., McGregor, K. C., & Bingner, R. L: User’s Guide—revised
1043 universal soil loss equation version 2 (RUSLE 2). USDA–Agricultural Research Service, Washington, DC., 2002.
1044
1045 Frieler, K., Lange, S., Piontek, F., Reyher, C. P. O., Schewe, J., Warszawski, L., Zhao, F., Chini, L., Denvil, S., Emanuel, K.,
1046 Geiger, T., Halladay, K., Hurtt, G., Mengel, M., Murakami, D., Ostberg, S., Popp, A. and Riva, R.: Assessing the impacts
1047 of 1.5 °C global warming – simulation protocol of the Inter-Sectoral Impact Model Intercomparison Project (ISIMIP2b),

1048 Geosci. Model Dev., 10, 4321–4345, 2017.

1049

1050 Galy, V., Peucker-Ehrenbrink, B., & Eglinton, T. Global carbon export from the terrestrial biosphere controlled by erosion.

1051 Nature, 521, 204–207. <https://doi.org/10.1038/nature14400>, 2015.

1052

1053 Guenet, B., Camino-Serrano, M., Ciais, P., Tifafi, M., Maignan, F., Soong, J. L., & Janssens, I. A.: Impact of

1054 priming on global soil carbon stocks, *Global change biology*, 24(5), 1873–1883, 2018.

1055

1056 Gumiere, S. J., Le Bissonnais, Y., Raclot, D., & Cheviron, B.: Vegetated filter effects on sedimentological connectivity of

1057 agricultural catchments in erosion modelling: a review. *Earth Surface Processes and Landforms*, 36(1), 3–19, 2011.

1058

1059 Hay R.K.M.: Harvest index: a review of its use in plant breeding and crop physiology, *Ann. appl. Biol.*, 126, 197–216,

1060 1995.

1061

1062 Hoffmann, T., Erkens, G., Cohen, K. M., Houben, P., Seidel, J. and Dikau, R.: Holocene floodplain sediment storage and

1063 hillslope erosion within the Rhine catchment, *The Holocene*, 17(1), 105–118, doi:10.1177/0959683607073287, 2007.

1064

1065 Hoffmann, T., Lang, a and Dikau, R.: Holocene river activity: analysing 14C-dated fluvial and colluvial sediments from

1066 Germany, *Quat. Sci. Rev.*, 27(21–22), 2031–2040, doi:10.1016/j.quascirev.2008.06.014, 2008.

1067

1068 Hoffmann, T., Schlummer, M., Notebaert, B., Verstraeten, G. and Korup, O.: Carbon burial in soil sediments from

1069 Holocene agricultural erosion, Central Europe, *Global Biogeochem. Cycles*, 27(3), 828–835, doi:10.1002/gbc.20071,

1070 2013a.

1071

1072 Hoffmann, T., Mudd, S. M., van Oost, K., Verstraeten, G., Erkens, G., Lang, a., Middelkoop, H., Boyle, J., Kaplan, J. O.,

1073 Willenbring, J. and Aalto, R.: Short Communication: Humans and the missing C-sink: erosion and burial of soil carbon

1074 through time, *Earth Surf. Dyn.*, 1(1), 45–52, doi:10.5194/esurf-1-45-2013, 2013b.

1075

1076 Hurtt, G. C., Chini, L. P., Frohking, S., Betts, R. A., Feddema, J. and Fischer, G.: Harmonization of land-use scenarios for

1077 the period 1500 – 2100 : 600 years of global gridded annual land-use transitions , wood harvest , and resulting secondary

1078 lands, *Clim. Chang.*, 109, 117–161, doi:10.1007/s10584-011-0153-2, 2011.

1079

1080 Kinnell, P. I. A.: Runoff dependent erosivity and slope length factors suitable for modelling annual erosion using the

1081 Universal Soil Loss Equation. *Hydrological Processes: An International Journal*, 21(20), 2681–2689, 2007.

1082

1083 Krinner, G., Viovy, N., de Noblet-Ducoudré, N., Ogée, J., Polcher, J., Friedlingstein, P., Ciais, P., Sitch, S. and Prentice, I.

1084 C.: A dynamic global vegetation model for studies of the coupled atmosphere-biosphere system, *Global Biogeochem.*
1085 *Cycles*, 19(1), 1–33, doi:10.1029/2003GB002199, 2005.

1086

1087 Lal, R.: Soil erosion and the global carbon budget., *Environ. Int.*, 29(4), 437–50, doi:10.1016/S0160-4120(02)00192-7,
1088 2003.

1089

1090 Lehner, B. and Grill, G.: Global river hydrography and network routing : baseline data and new approaches to study the
1091 world ' s large river systems, *Hydrol. Process.*, 2186(April), 2171–2186, doi:10.1002/hyp.9740, 2013.

1092

1093 Li, L., Ni, J., Chang, F., Yue, Y., Frolova, N., Magritsky, D., Borthwick, A.G., Ciais, P., Wang, Y., Zheng, C. and Walling,
1094 D.E.: Global trends in water and sediment fluxes of the world's large rivers, *Science Bulletin*, 65(1), 62-69,
1095 doi:10.1016/j.scib.2019.09.012, 2020.

1096

1097 Ludwig, W. and Probst, J.-L.: River Sediment Discharge to the Oceans: Present-Day Controls and Global Budgets, *Am. J.*
1098 *Sci.*, 298(April), 265–295, 1998.

1099

1100 Lugato, E., Smith, P., Borrelli, P., Panagos, P., Ballabio, C., Orgiazzi, A., Fernandez-ugalde, O., Montanarella, L. and
1101 Jones, A.: Soil erosion is unlikely to drive a future carbon sink in Europe, *Scientific Advances*, 4(November), eaau3523,
1102 2018.

1103

1104 Martínez-mena, M., Almagro, M., García-franco, N., Vente, J. De and García, E.: Fluvial sedimentary deposits as carbon
1105 sinks : organic carbon pools and stabilization mechanisms across a Mediterranean catchment, *Biogeosciences* 16,
1106 1035–1051, 2019.

1107

1108 Mayorga, E., Seitzinger, S. P., Harrison, J. a., Dumont, E., Beusen, A. H. W., Bouwman, a. F., Fekete, B. M., Kroeze, C.
1109 and Van Drecht, G.: Global Nutrient Export from WaterSheds 2 (NEWS 2): Model development and implementation,
1110 *Environ. Model. Softw.*, 25(7), 837–853, doi:10.1016/j.envsoft.2010.01.007, 2010.

1111

1112 Müller, C., Elliott, J., Kelly, D., Arneth, A., Balkovic, J., Ciais, P., ... & Jones, C. D.: The Global Gridded Crop Model
1113 Intercomparison phase 1 simulation dataset, *Scientific data*, 6(1), 50, 2019.

1114

1115 Nadeu, E., Gobin, A., Fiener, P., van Wesemael, B. and van Oost, K.: Modelling the impact of agricultural management on
1116 soil carbon stocks at the regional scale: the role of lateral fluxes., *Glob. Chang. Biol.*, 21(8), 3181–92,
1117 doi:10.1111/gcb.12889, 2015.

1118

1119 Naipal, V., Reick, C., Pongratz, J. and Van Oost, K.: Improving the global applicability of the RUSLE model - Adjustment

1120 of the topographical and rainfall erosivity factors, *Geosci. Model Dev.*, 8(9), doi:10.5194/gmd-8-2893-2015, 2015.

1121

1122 Naipal, V., Reick, C., Van Oost, K., Hoffmann, T. and Pongratz, J.: Modeling long-term, large-scale sediment storage using
1123 a simple sediment budget approach, *Earth Surf. Dyn.*, 4, 407–423, doi:10.5194/esurf-4-407-2016, 2016.

1124

1125 Naipal, V., Ciais, P., Wang, Y., Lauerwald, R., Guenet, B. and Oost, K. Van: Global soil organic carbon removal by water
1126 erosion under climate change and land use change during AD 1850 – 2005, *Biogeosciences*, 15(July), 4459–4480,
1127 doi:<https://doi.org/10.5194/bg-15-4459-2018>, 2018.

1128

1129 Van Oost, K., Quine, T. a, Govers, G., De Gryze, S., Six, J., Harden, J. W., Ritchie, J. C., McCarty, G. W., Heckrath, G.,
1130 Kosmas, C., Giraldez, J. V, da Silva, J. R. M. and Merckx, R.: The impact of agricultural soil erosion on the global carbon
1131 cycle., *Science*, 318(5850), 626–9, doi:10.1126/science.1145724, 2007.

1132

1133 Van Oost, K., Verstraeten, G., Doetterl, S., Notebaert, B., Wiaux, F. and Broothaerts, N.: Legacy of human-induced C
1134 erosion and burial on soil – atmosphere C exchange, *PNAS*, 109(47), 19492–19497,
1135 doi:10.1073/pnas.1211162109/-/DCSupplemental.www.pnas.org/cgi/doi/10.1073/pnas.1211162109, 2012.

1136

1137 Palmieri, A., Martino, L., Dominici, P. and Kasanko, M.: Land Cover and Land Use Diversity Indicators in LUCAS 2009
1138 data., 2011.

1139

1140 Panagos, P., Borrelli, P., Poesen, J., Ballabio, C., Lugato, E., Meusburger, K., Montanarella, L. and Alewell, C.:
1141 Environmental Science & Policy The new assessment of soil loss by water erosion in Europe, *Environ. Sci. Policy*, 54,
1142 438–447, doi:10.1016/j.envsci.2015.08.012, 2015.

1143

1144 Panagos, P., Borrelli, P., Meusburger, K., Yu, B., Klik, A., Lim, K. J., Yang, J. E., Ni, J., Miao, C., Chattopadhyay, N.,
1145 Sadeghi, S. H., Hazbavi, Z., Zabihi, M., Larionov, G. A., Krasnov, S. F., Gorobets, A. V., Levi, Y., Erpul, G., Birkel, C.,
1146 Hoyos, N., Naipal, V., Oliveira, P. T. S., Bonilla, C. A., Meddi, M., Nel, W., Al Dashti, H., Boni, M., Diodato, N., Van
1147 Oost, K., Nearing, M. and Ballabio, C.: Global rainfall erosivity assessment based on high-temporal resolution rainfall
1148 records, *Sci. Rep.*, 7(1), doi:10.1038/s41598-017-04282-8, 2017.

1149

1150 Parton, W. J., Schimel, D. S., Cole, C. V. and Ojima, D. S.: Analysis of Factors Controlling Soil Organic Matter Levels in
1151 Great Plains Grasslands1, *Soil Sci. Soc. Am. J.*, 51(5), 1173, doi:10.2136/sssaj1987.03615995005100050015x, 1987.

1152

1153 Pelletier, J. D.: A spatially distributed model for the long-term suspended sediment discharge and delivery ratio of drainage
1154 basins, *J. Geophys. Res., Earth Surface* 117 (F2), doi: <https://doi.org/10.1029/2011JF002129>, 2012.

1155
1156 Pelletier, J. D., Broxton, P. D., Hazenberg, P., Zeng, X., Troch, P. A., Niu, G. Y., Williams, Z., Brunke, M. A. and Gochis,
1157 D.: A gridded global data set of soil, intact regolith, and sedimentary deposit thicknesses for regional and global land
1158 surface modeling, *J. Adv. Model. Earth Syst.*, doi:10.1002/2015MS000526, 2016.
1159
1160 Peng, S., Ciais, P., Maignan, F., Li, W., Chang, J., Wang, T. and Yue, C.: Sensitivity of land use change emission estimates
1161 to historical land use and land cover mapping, *Global Biogeochem. Cycles*, 31(4), 626–643, doi:10.1002/2015GB005360,
1162 2017.
1163
1164 Renard, K. G., & Ferreira, V. A.: RUSLE model description and database sensitivity. *Journal of environmental quality*,
1165 22(3), 458-466, 1993.
1166
1167 Renard, K.G., Foster, G.R., Weesies, G.A., McCool, D.K., Yoder, D. C.: *Predicting Soil Erosion by Water: A Guide to*
1168 *Conservation Planning with the Revised Universal Soil Loss Equation (RUSLE)*, United States Department of Agriculture,
1169 Washington, DC., 1997.
1170
1171 *Van Rompaey, A.J., Verstraeten, G., Van Oost, K., Govers, G. and Poesen, J.: Modelling mean annual sediment yield using*
1172 *a distributed approach, Earth Surface Processes and Landforms*, 26(11), 1221-1236, 2001.
1173
1174 Schauburger, B., Ben-ari, T., Makowski, D., Kato, T., Kato, H. and Ciais, P.: Yield trends , variability and stagnation
1175 analysis of major crops in France over more than a century, *Sci. Rep.*, (November), 1–12,
1176 doi:10.1038/s41598-018-35351-1, 2018.
1177
1178 Shangguan H.W., Dai Y., Duan Q., Liu B., Y. H.: A global soil data set for earth system modeling *Wei, J. Adv. Model.*
1179 *Earth Syst.*, 6, 249–263, 2014, doi:10.1002/2013MS000293.
1180
1181 Sorribas, M. V., da Motta Marques, D., Castro, N. M. D. R., & Fan, F. M.: Fluvial carbon export and CO2 efflux in
1182 representative nested headwater catchments of the eastern La Plata River Basin, *Hydrological processes*, 31(5), 995-1006,
1183 2017.
1184
1185 Stallard, R. F.: Terrestrial sedimentation and the carbon cycle : Coupling weathering and erosion to carbon burial, *Global*
1186 *Biogeochem. Cycles*, 12(2), 231–257, 1998.
1187
1188 Tan, Z., Leung, L. R., Li, H., Tesfa, T., Vanmaercke, M., Poesen, J., ... Hartmann, J. A Global data analysis for representing
1189 sediment and particulate organic C carbon yield in Earth System Models. *Water Resources Research*, 53, 10,674–10,700.
1190 <https://doi.org/10.1002/2017WR020806>, 2017

1191
1192 Thonicke, K., Spessa, A., Prentice, I. C., Harrison, S. P. and Dong, L.: The influence of vegetation , fire spread and fire
1193 behaviour on biomass burning and trace gas emissions: results from a process-based model, *Biogeosciences*, 7,
1194 1991–2011, doi:10.5194/bg-7-1991-2010, 2010.
1195
1196 Todd-Brown, K. E., Randerson, J. T., Post, W. M., Hoffman, F. M., Tarnocai, C., Schuur, E. A., & Allison, S. D.: Causes of
1197 variation in soil carbon simulations from CMIP5 Earth system models and comparison with observations, *Biogeosciences*
1198 (10), 1717-1736, 10.5194/bg-10-1717-2013, 2013.
1199
1200 Wang, Z., Govers, G., Steegen, A., Clymans, W., Putte, A. Van Den, Langhans, C., Merckx, R. and Oost, K. Van:
1201 Geomorphology Catchment-scale carbon redistribution and delivery by water erosion in an intensively cultivated area,
1202 *Geomorphology*, 124(1–2), 65–74, doi:10.1016/j.geomorph.2010.08.010, 2010.
1203
1204 Wang, Z., Doetterl, S., Vanclooster, M., van Wesemael, B. and Van Oost, K.: Constraining a coupled erosion and soil
1205 organic carbon model using hillslope-scale patterns of carbon stocks and pool composition, *J. Geophys. Res.*
1206 *Biogeosciences*, 120, 452–465, doi:10.1002/2014JG002768, 2015.
1207
1208 Wang, Z., Hoffmann, T., Six, J., Kaplan, J. O., Govers, G., Doetterl, S. and Van Oost, K.: Human-induced erosion has
1209 offset one-third of carbon emissions from land cover change, *Nat. Clim. Chang.*, 7(5), 345–349, doi:10.1038/nclimate3263,
1210 2017.
1211
1212 Wiesmeier, M., Sporlein, P., Geuß, U. W. E., Hangen, E., Haug, S., Reischl, A., Schilling, B., Lutzow, M. V. O. N. and
1213 Kogel-Knaber, I.: Soil organic carbon stocks in southeast Germany (Bavaria) as affected by land use , soil type and
1214 sampling depth, *Glob. Chang. Biol.*, (March), 1–13, doi:10.1111/j.1365-2486.2012.02699.x, 2012.
1215
1216
1217
1218
1219
1220
1221
1222
1223
1224
1225
1226

Table 1: Model input datasets

Dataset	Spatial resolution	Temporal resolution	Period	Source
Historical land cover and land use change	0.25 degrees	annual	1850-2005	Peng et al. (2017)
Climate data (precipitation & temperature) for ORCHIDEE	0.5 degrees	6 hourly	1900-2012	CRU-NCEP version 5.3.2; https://crudata.uea.ac.uk/cru/data/ncep/ ; last access: 5 April 2019
precipitation for the Adj. RUSLE	0.5 degrees	monthly	1850-2005	ISIMIP2b (Frieler et al., 2017)
Soil	1 km	-	-	Global Soil Dataset for Earth System Modeling, GSDE (Shangguan H.W., Dai Y., Duan Q., Liu B., 2014)
Topography	30 arcseconds	-	-	GTOPO30; U.S. Geological Survey, EROS Data Center Distributed Active Archive Center 2004; https://www.ngdc.noaa.gov/mgg/topo/gltiles.html ; last access: 5 April 2019
Flow accumulation	30 arcseconds	-	-	HydroSHEDS (Lehner et al., 2013); https://www.hydrosheds.org/ ; last access: 5 April 2019
Hillslopes/Floodplain area	5 arcminutes	-	-	Pelletier et al. (2016)
River network & stream length	30 arcseconds	-	-	Hydrosheds (Lehner et al., 2008)

1228

1229 **Table 2:** Model simulations, with changes to the basin average gross soil erosion rate ($t\ ha^{-1}\ y^{-1}$), the basin average
 1230 sediment residence time Tau (years), and the enrichment factor, and the crop residue harvest intensity, RM (%).

Default simulations	Gross soil erosion	Tau	Enrichment factor	RM
S0	0	-	-	0
S1	3.94	94	1	0
S2	3.94	94	1	0
Uncertainty simulations				
S1_min	1.52	94	1	0
S2_min	1.52	94	1	0

S1_max	5.95	94	1	0
S2_max	5.95	94	1	0
Sensitivity simulations				
S2_Tmin	3.94	60	1	0
S2_Tmax	4.94	128	1	0
S1_EF	5.94	94	2	0
S2_EF	6.94	94	2	0
S0_RM	0	-	-	100
S1_RM	3.94	94	1	100
S2_RM	3.94	94	1	100

1231
1232 **Table 3:** Goodness-of-fit results of the comparison of the simulated gross and net erosion rates to those of other studies at
1233 subbasin level, taking into account 13 sub-basins of the Rhine. RMSE is the root mean square error in 10^6 tons year⁻¹. E
1234 stands for soil erosion.

	E Cerdan et al. (2010)	E Germany	E RUSLE2015	E Borrelli et al. (2018)
<i>r-squared</i>	0.72	0.97	0.94	0.24
<i>RMSE</i>	0.68	1.98	0.92	1.35

1235
1236 **Table 4:** Goodness-of-fit results of the comparison of the simulated gross and net C erosion rates to those of the study of
1237 Lugato et al. (2018) in the enhanced and reduced scenario, taking into account 13 sub-basins of the Rhine. RMSE is the
1238 root mean square error in tons year⁻¹. Ce stands for gross C erosion, while Cd stands for net C erosion.

	Ce enhanced	Ce reduced	Cd enhanced	Cd reduced
<i>r-squared</i>	0.95	0.95	0.98	0.98
<i>RMSE</i>	7977	13797	3450	9822

1239
1240 **Table 5:** This table shows the results of the linear regression between the simulated total SOC stocks (Tg of C per year)
1241 and those of the Global Soil dataset for Earth System Modeling (GSDE) and from the LUCAS database. The regression is
1242 done after aggregating the data at sub-basin level for the 13 sub-basins that were delineated in the Rhine catchment.
1243 RMSE is the root mean square error given in Tg of C per year, while the r-value is the spatial correlation coefficient.

Regression	r-value	p-value	RMSE
------------	---------	---------	------

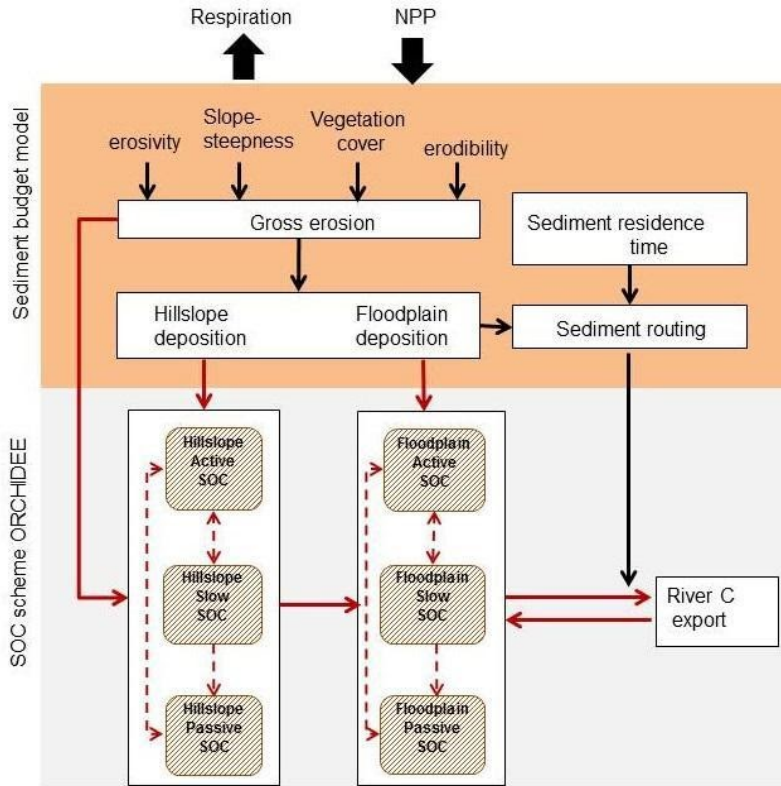
This study versus LUCAS	0.96	<0.01	28.69
This study versus GSDE	0.95	<0.01	29.32

1244
1245 **Table 6:** This table presents the scaling exponent (b) of equation 20 for floodplains and hillslopes. The scaling exponent
1246 was derived for selected points in the Rhine catchment for which measurements on the SOC storage were taken by
1247 Hoffmann et al. (2013), and at sub-basin level after the data on area and SOC stocks was aggregated for each of the 13
1248 sub-basins of the Rhine.

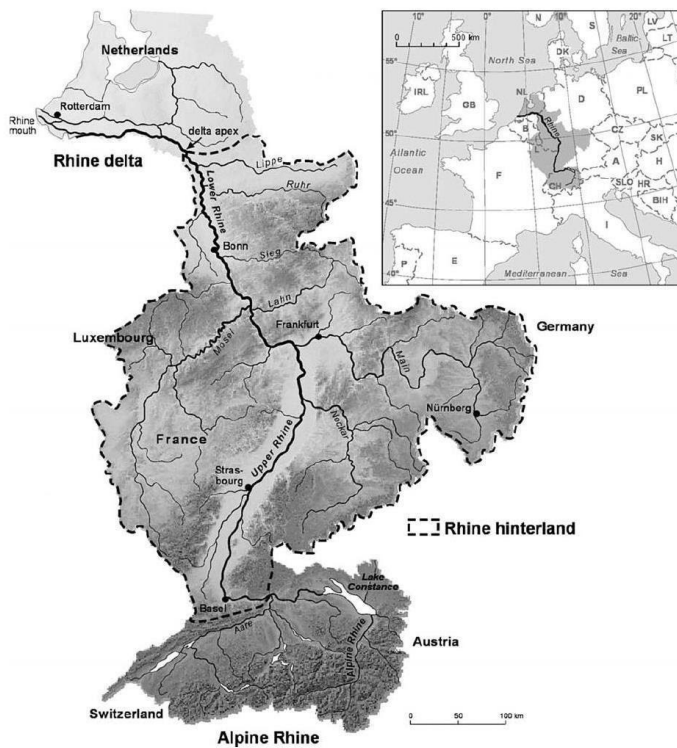
	Scaling exponent floodplains	Scaling exponent hillslopes
Hoffmann et al. (2013)	1.23±0.06	1.08±0.07
This study (selected points where measurements were taken)	1.14	0.83
This study (based on the 13 sub-basins)	1.06	1.00

1249
1250 **Table 7:** Sensitivity analysis. The impacts of enrichment, changes to the sediment residence time (τ_{min} , τ_{max}), and crop
1251 residue management (RM) on the cumulative gross C erosion (C_e), the cumulative change in the total SOC stock ($dSOC$), the
1252 net C sink and the cumulative particulate organic C export flux (POC_{exp}) of the Rhine catchment. Units: Tg C

	C_e	dSOC	C sink/source	POC_{exp}
Default	66	142	216	0.029138
enrichment	106	198	271	0.032137
τ_{min}	66	130	204	0.026198
τ_{max}	66	100	173	0.036117
RM	52	105	194	0.031134

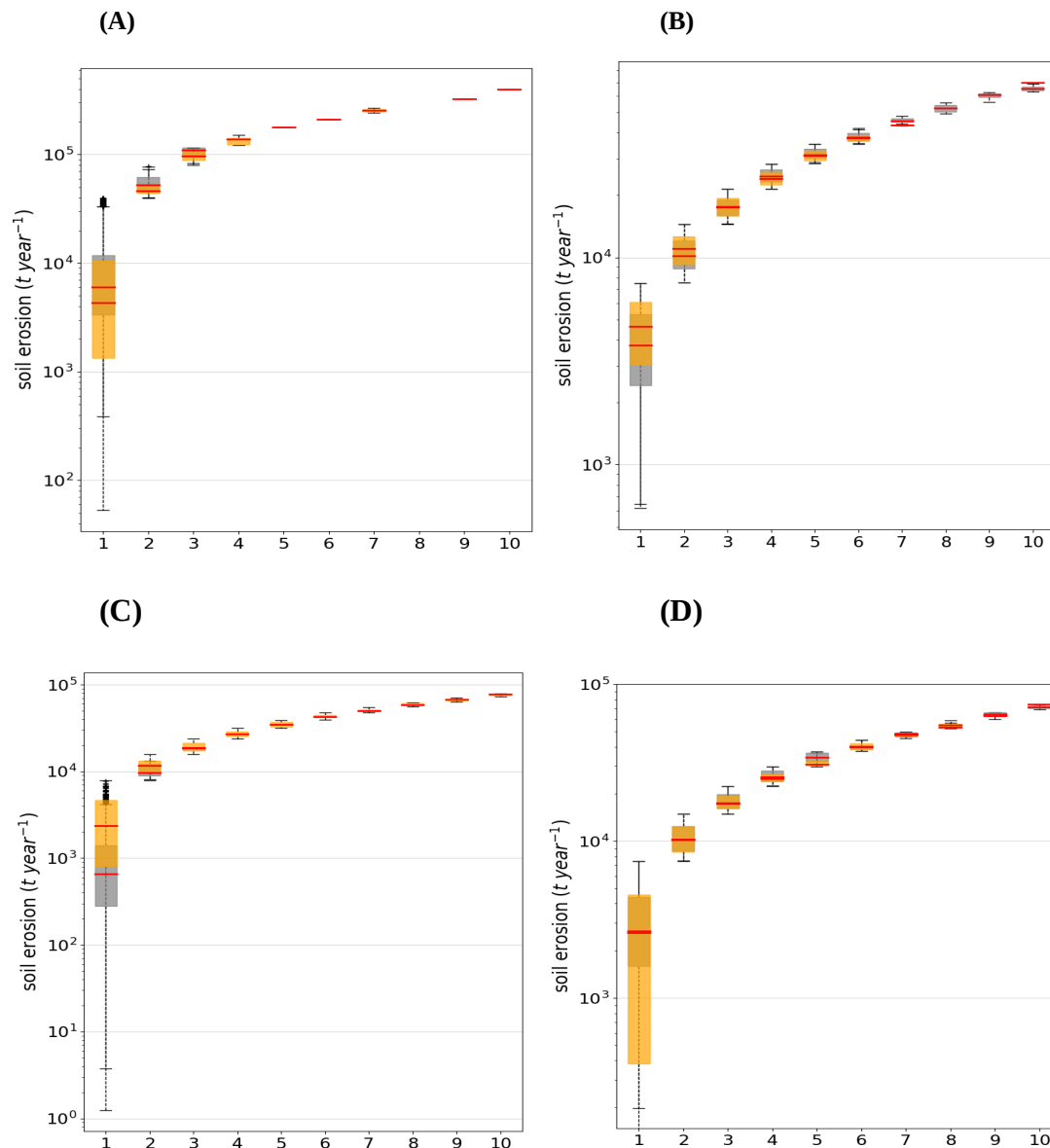


1255 **Figure 1:** A conceptual diagram of CE-DYNAM. The red arrows represent the C fluxes between the C pools/reservoirs,
 1256 while the black arrows represent the link between the erosion processes (removal, deposition and transport).
 1257



1258 **Figure 2:** The Rhine catchment (Hoffmann et al., 2013), where the gray shades represent elevation and the continuous
1259 black lines the main rivers.

1260
1261



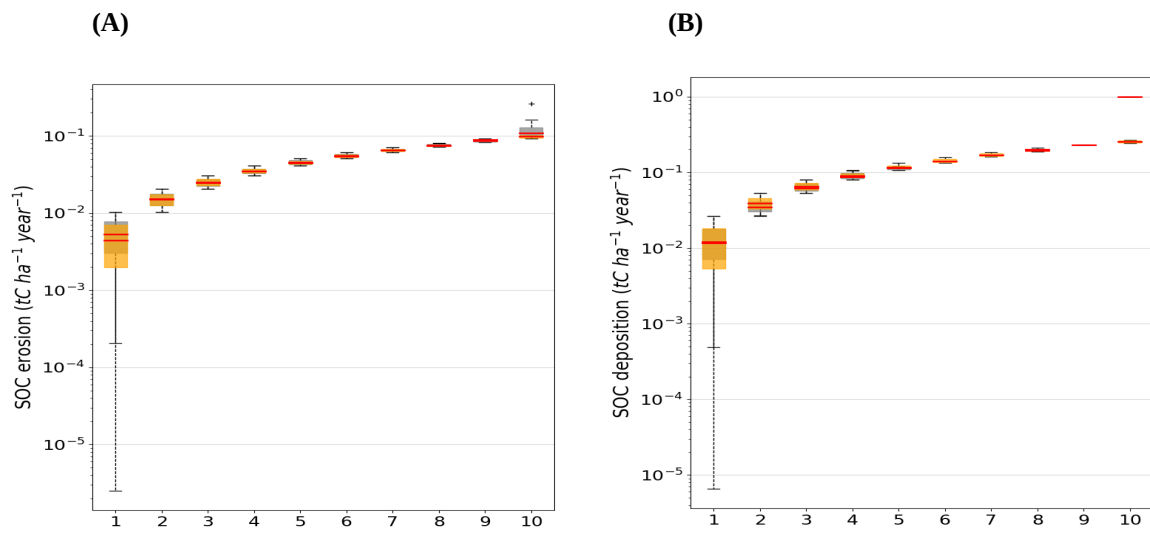
1262
1263

1264 **Figure 3:** Quantile-whisker plot of simulated **gross** soil erosion rates (t/year) (grey whisker boxes), compared to (A) the
1265 study of Cerdan et al. (2010), (B) the study of Panagos et al. (2015), and (C) the German potential erosion map by Bug et
1266 al. (2014) (orange whisker boxes). (D) Quantile-whisker plot of simulated **net** soil erosion rates (t/year) (grey whisker
1267 boxes), compared to the study of Borrelli et al. (2018) (orange whisker boxes). Medians are plotted as red horizontal lines.
1268 The x-axis represents bins or evenly spaced ranges between the minimum and maximum total yearly soil erosion rates of
1269 the Rhine derived from the data of (a) Cerdan et al. (2010), (b) Panagos et al. (2015), (c) Bug et al. (2014), and (d) Borrelli
1270 et al. (2018). The x-axis represents bins or evenly spaced ranges between the minimum and maximum total yearly soil
1271 erosion rates of the Rhine.

1272

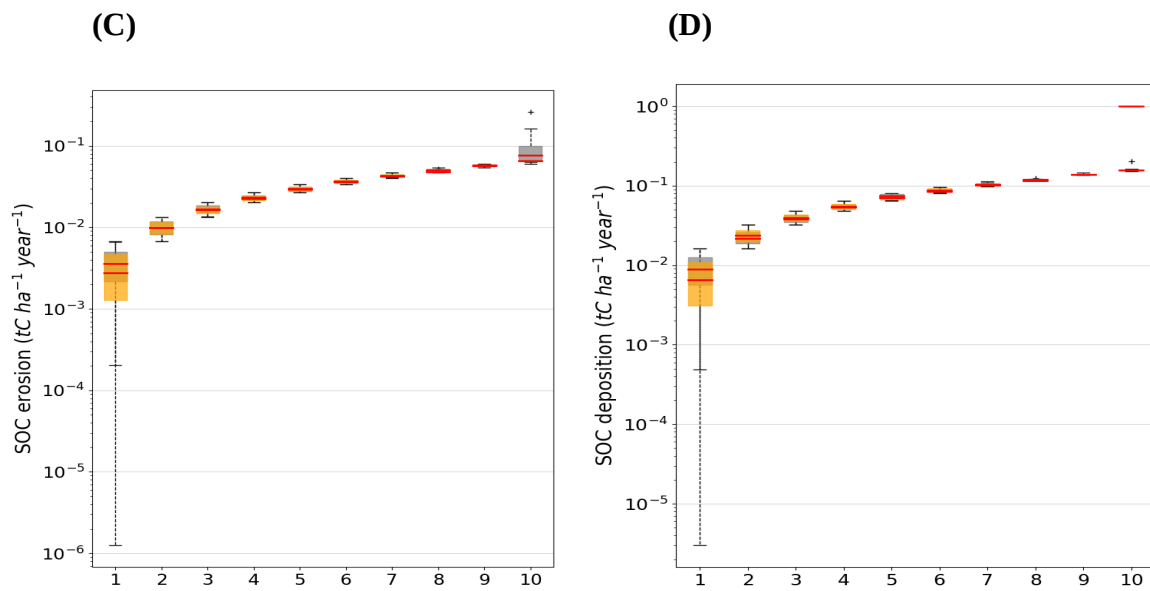
1273

1274



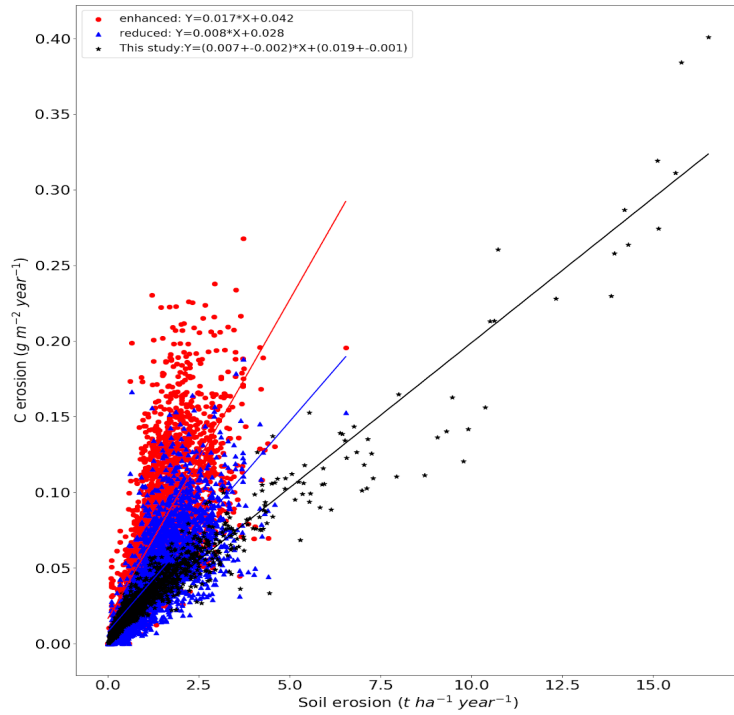
1275

1276



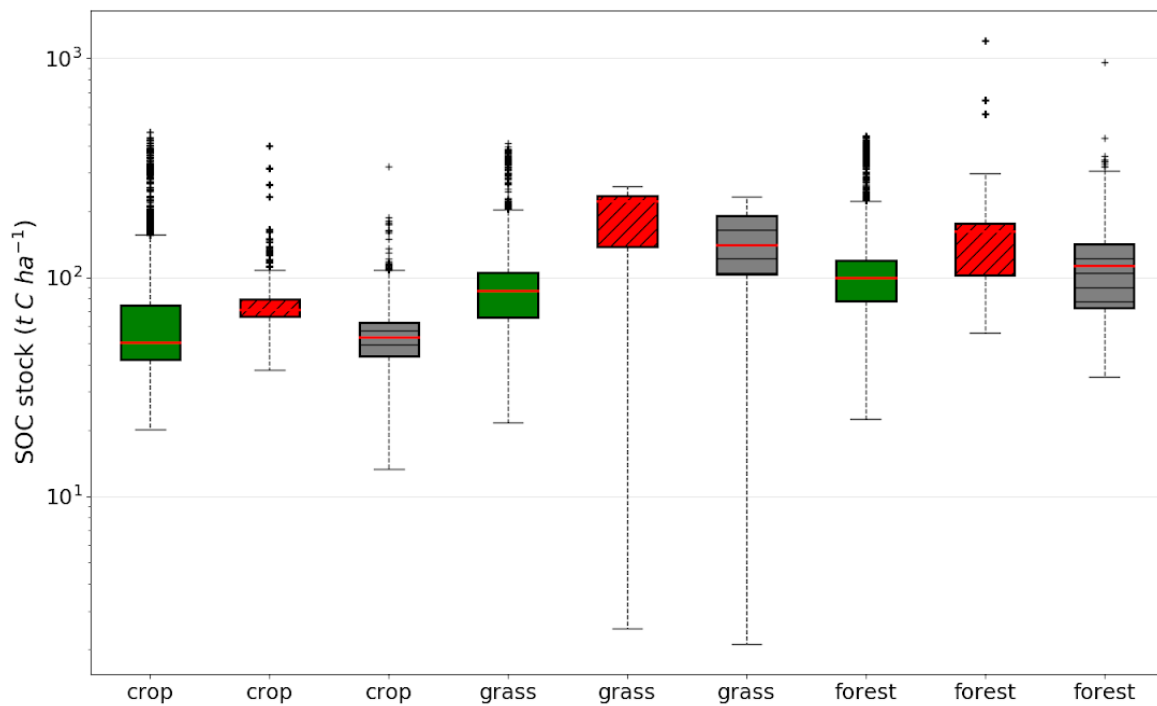
1277 **Figure 4:** (A) Hillslope C erosion rates and, (B) C deposition rates, compared to the enhanced erosion scenario from
1278 Lugato et al. (2018). (C) Hillslope C erosion rates and, (D) C deposition rates, compared to the reduced erosion scenario
1279 from Lugato et al. (2018). The x-axis represents bins or evenly spaced ranges between the minimum and maximum total
1280 yearly soil erosion rates of the Rhine.

1281



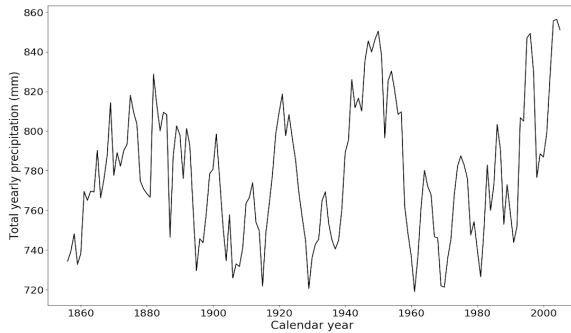
1282 **Figure 5:** The relationship between soil erosion and C erosion of simulation S2 (blackstars) in comparison to the erosion
1283 scenarios from the study of Lugato et al. (2018) with enhanced (red circles) and reduced erosion (blue triangles),
1284 respectively. The straight lines are the trendlines of the linear regression between soil and C erosion.

1285

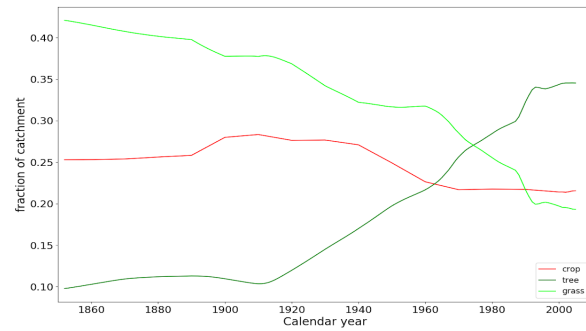


1286 **Figure 6:** Comparison of the total SOC stocks per land cover type between the simulation without erosion (red boxes with
 1287 a ‘//’ pattern), the simulation with erosion (black boxes with a ‘-’ pattern) and the LUCAS data (green boxes without
 1288 pattern fill). The red horizontal lines are the medians, the dashed vertical lines represent the range between the minimum
 1289 and maximum, and the black dots are the outliers.

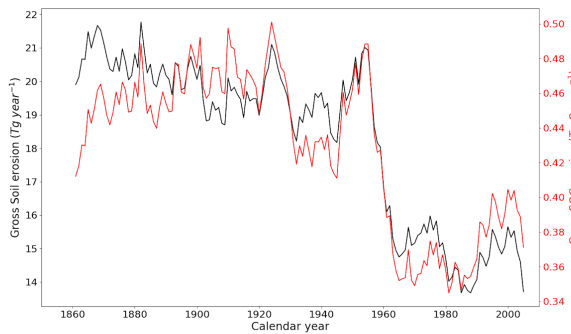
1290 (A)
 1291



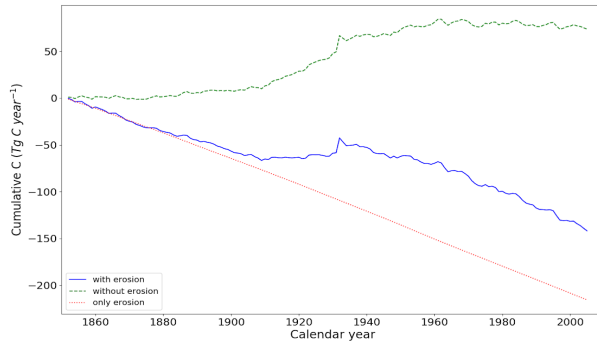
(B)



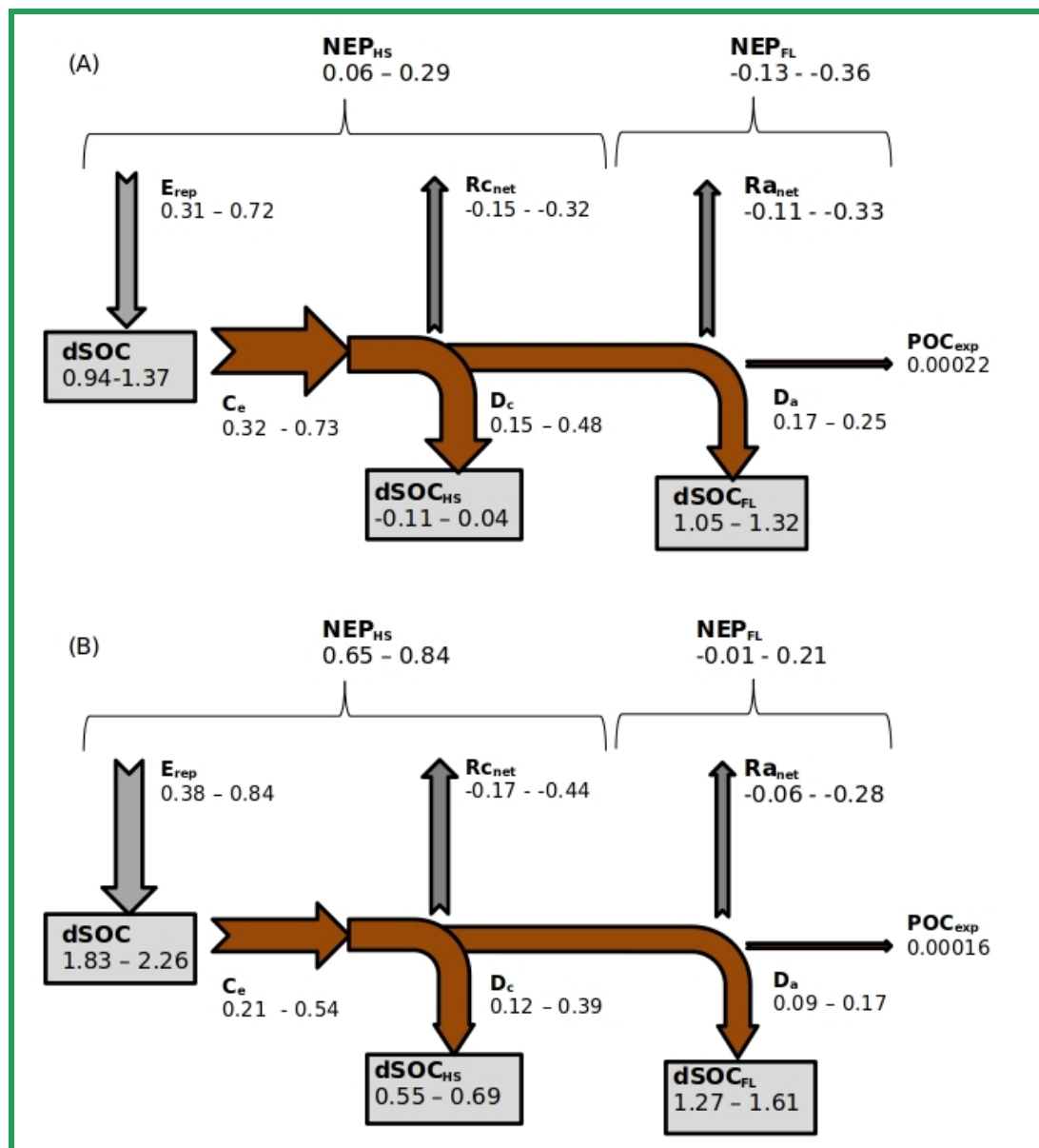
1292 (C)
 1293

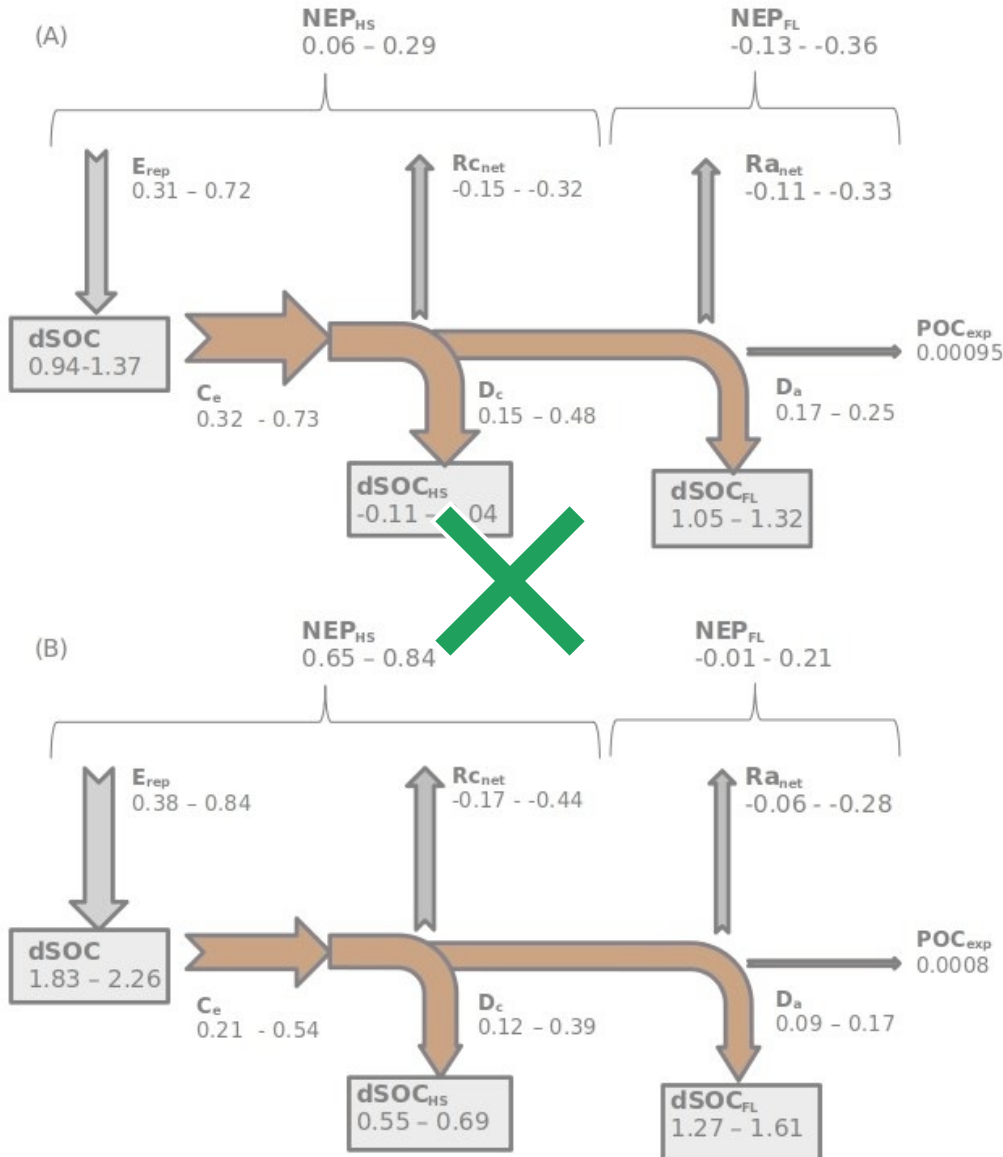


(D)



1294 **Figure 7:** Timeseries of (A) the 5-year average yearly precipitation (mm), (B) changing land cover fractions, (C): 5-year
 1295 average total gross soil erosion (Pg year^{-1}) and total gross C erosion rates (Tg C year^{-1}), (D): Cumulative C emissions from
 1296 the soil to the atmosphere under land use change and climate change without soil erosion (green dashed line), with soil
 1297 erosion (blue straight line), due to additional respiration or stabilization of buried soil and photosynthetic replacement of C
 1298 under erosion (E_p , red dotted line). All graphs represent the non-Alpine region of the Rhine catchment.

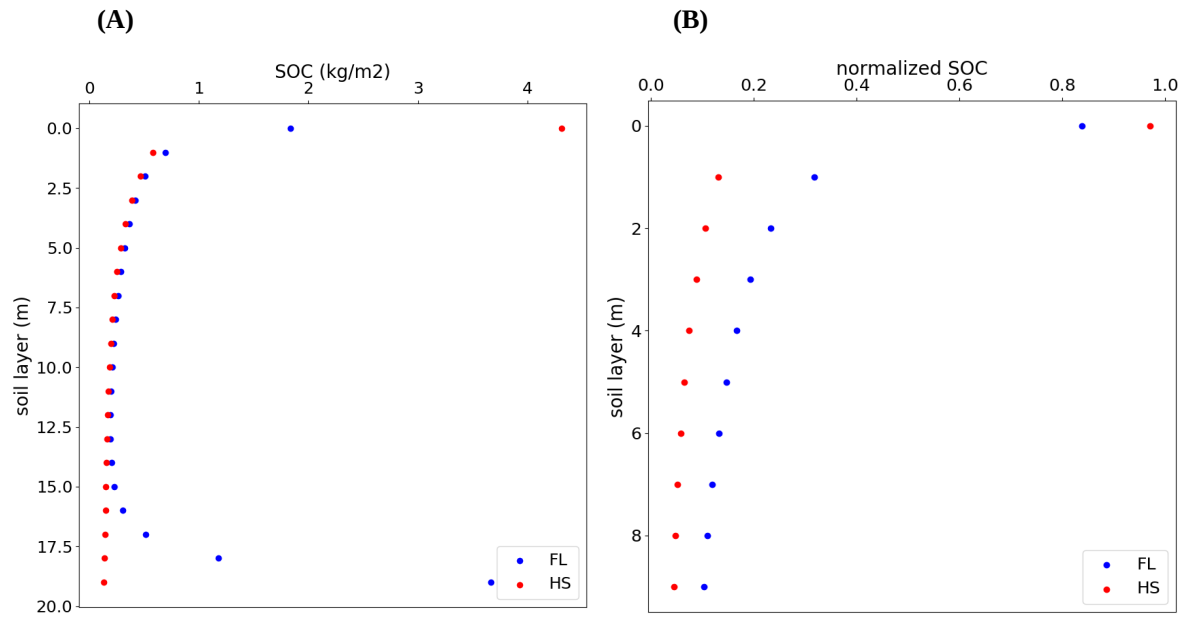




1300 **Figure 8:** (A) C budget of the non-Alpine part of the Rhine for the period 1851-1861, and (B) for the period 1995-2005.
 1301 The budget shows the net exchange of C ($Tg\ C\ year^{-1}$) between the soil and atmosphere as a result of accelerated soil
 1302 erosion rates. Grey arrows are the erosion-induced yearly average **vertical** C fluxes, while the brown arrows are the
 1303 erosion-induced yearly average **lateral** C fluxes. C_e : Gross C erosion from hillslopes; D_c : Deposition of C on hillslopes;
 1304 D_a : Deposition of C in floodplains; POC_{exp} : net POC export flux; E_p : Erosion-induced C replacement on hillslopes (Eq. 21);
 1305 $R_{a_{net}}$: Net respiration/burial of deposited C in floodplains (Eq. 23); $R_{c_{net}}$: Net respiration/burial of deposited C on hillslopes
 1306 (Eq. 22); NEP_{HS} : Net ecosystem productivity of hillslopes; NEP_{FL} : Net ecosystem productivity of floodplains; The grey
 1307 boxes represent yearly average changes in SOC stocks for the specific time period as a result of land use change, climate
 1308 change, erosion and deposition. $dSOC$: Yearly average change in the total SOC stock; $dSOC_{HS}$: Yearly average change in
 1309 the hillslope SOC stock; $dSOC_{FL}$: Yearly average change in the floodplain SOC stock.

1310

1311



1312

1313

1314

Figure 9: (A) Vertical distribution of hillslope (red) and floodplain (blue) SOC stocks (kg m^{-2}) with depth averaged over the non-Alpine region of the Rhine catchment, and (B) the vertical distribution of normalized hillslope (red) and floodplain (blue) SOC stocks (dimensionless) with depth.